JEM Journal of Experimental Medicine

ARTICLE

Endothelial IQGAP1 regulates leukocyte transmigration by directing the LBRC to the site of diapedesis

David P. Sullivan[1], Prarthana J. Dalal[1], Fanny Jaulin[2], David B. Sacks[3], Geri Kreitzer[4], and William A. Muller[1]

Transendothelial migration (TEM) of leukocytes across the endothelium is critical for inflammation. In the endothelium, TEM requires the coordination of membrane movements and cytoskeletal interactions, including, prominently, recruitment of the lateral border recycling compartment (LBRC). The scaffold protein IQGAP1 was recently identified in a screen for LBRC-interacting proteins. Knockdown of endothelial IQGAP1 disrupted the directed movement of the LBRC and substantially reduced leukocyte TEM. Expression of truncated IQGAP1 constructs demonstrated that the calponin homology domain is required for IQGAP1 localization to endothelial borders and that the IQ domain, on the same IQGAP1 polypeptide, is required for its function in TEM. This is the first reported function of IQGAP1 requiring two domains to be present on the same polypeptide. Additionally, we show for the first time that IQGAP1 in the endothelium is required for efficient TEM in vivo. These findings reveal a novel function for IQGAP1 and demonstrate that IQGAP1 in endothelial cells facilitates TEM by directing the LBRC to the site of TEM.

Introduction

Inflammation evolved to eliminate pathogens, resolve injury, and return the body to homeostasis. However, when improperly regulated, whether overstimulated (reperfusion injury) or self-directed (arthritis [Firestein and McInnes, 2017] and multiple sclerosis [Grigoriadis et al., 2015]), uncontrolled inflammation becomes pathological. One of the critical steps in mounting an effective inflammatory response is the recruitment of various leukocytes to the site of inflammation, and thus, this represents an attractive therapeutic target to reduce untoward inflammation (Muller, 2016a,b).

Leukocyte recruitment involves a complex cascade of sequential adhesive and signaling steps that culminate in the migration of the leukocyte across the vascular endothelium through a process commonly referred to as diapedesis or transendothelial cell migration (TEM; Gerhardt and Ley, 2015; Muller, 2016b). The process requires coordinated movements of plasmalemmal and vesicular membrane, rapid and reversible changes in composition of adhesion molecules at junctional contacts, and local rearrangements of cytoskeletal elements. The lateral border recycling compartment (LBRC) of endothelial cells solves many of these problems. The LBRC is a subjunctional reticulum of interconnected tubulovesicular membrane that constitutively cycles to and from the endothelial cell border with a half-time of ∼10 min (Mamdouh et al., 2003). During TEM, membrane from the LBRC is targeted to the site of TEM along microtubules (Mamdouh et al., 2008) by Kinesin-1/KLC1c molecular motors (Cyrus and Muller, 2016), bringing increased membrane surface area containing platelet endothelial cell adhesion molecule (PECAM), poliovirus receptor, CD99, and other positive regulators of TEM (Muller, 2011; Sullivan et al., 2013; Sullivan and Muller, 2014) while displacing structural elements of the junctions such as vascular endothelial cadherin (VE-cadherin; Gonzalez et al., 2016) and Claudin-5 (Winger et al., 2014). Our laboratory demonstrated that endothelial cell PECAM and CD99 regulate TEM using distinct signaling pathways to recruit the LBRC (Watson et al., 2015; Weber et al., 2015). Recruitment of the LBRC seems to be the final common pathway for TEM; anything that interferes with the targeted recruitment of the LBRC to the leukocyte blocks TEM and reduces inflammation (Mamdouh et al., 2008; Dasgupta et al., 2009; Watson et al., 2015; Weber et al., 2015; Gonzalez et al., 2016). Yet, how the endothelial cell coordinates transmembrane signaling,

[1]Department of Pathology, Feinberg School of Medicine, Northwestern University, Chicago, IL; [2]Gustave Roussy Institute, Villejuif, France; [3]Department of Laboratory Medicine, National Institutes of Health, Bethesda, MD; [4]Department of Molecular, Cellular and Biomedical Sciences, City University of New York School of Medicine, The City College of New York, New York, NY.

Correspondence to William A. Muller: wamuller@northwestern.edu.

cytoskeletal rearrangements, and membrane movements to facilitate leukocyte infiltration remains a mystery.

Because the LBRC plays such a pivotal role in TEM, we isolated the compartment and characterized its protein components to gain insight into its regulation (Sullivan et al., 2014). The LBRC contains a representative sample of membrane proteins present at the lateral border of the endothelial cells (Feng et al., 2015). However, a cytosolic protein, IQ-motif–containing GTPase activating protein 1 (IQGAP1) was one of the few proteins enriched in membrane fractions containing the LBRC (Sullivan et al., 2014), leading us to examine if this protein plays a role in regulating either the structure or function of the LBRC.

IQGAP1 is a large multidomain cytosolic scaffolding protein that is involved in numerous seemingly disparate processes, including angiogenesis, cell proliferation, migration, adhesion, and tumorigenesis (reviewed in Abel et al., 2015; Hedman et al., 2015). Consistent with a role in these diverse processes, IQGAP1 has been shown to interact with well over 100 different signaling and cytoskeletal proteins (White et al., 2012; Hedman et al., 2015). The microtubule-binding proteins CLIP-170 and EB1, which bind IQGAP1 through its RasGAP C-terminal domain (Watanabe et al., 2004; Tian et al., 2014; Cao et al., 2015), are of particular interest in the context of TEM, since microtubules are critical for targeted recycling of the LBRC (Mamdouh et al., 2008; Cyrus and Muller, 2016). Furthermore, IQGAP1 homodimerization is believed to be important for its function (Bashour et al., 1997; Fukata et al., 1997; Mateer et al., 2002; Ren et al., 2005), at least under some conditions.

Despite numerous studies showing that IQGAP1 acts to coordinate multiple biological processes, its function as part of the LBRC is not known. There is only a single publication reporting a diminution in lymphocyte TEM in vitro when IQGAP1 was knocked down in endothelial cells. However, the mechanism for this phenomenon was, in retrospect, partially mischaracterized (Nakhaei-Nejad et al., 2010). Based on its association with the LBRC, we suspected that IQGAP1 may be a key molecule regulating TEM. The findings presented here show that IQGAP1 is required for targeted recycling of the LBRC during monocyte TEM. Furthermore, we show that the actin-binding calponin homology (CH) domain and the IQ domain must be on the same IQGAP1 molecule in order to function during TEM, but surprisingly, the microtubule-associating RasGAP C-terminal domain is not required. Most importantly, using bone marrow chimeras, we provide the first demonstration of the requirement for endothelial cell IQGAP1 in vivo in two models of inflammation, including intravital imaging in the cremaster muscle.

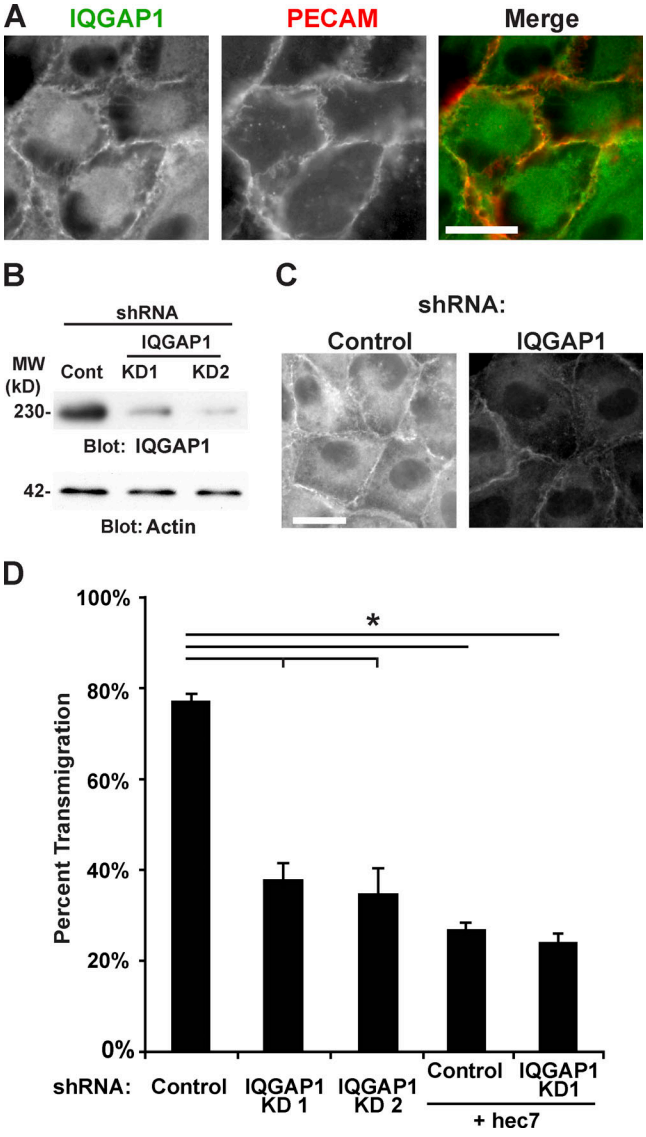

Figure 1. **IQGAP1 knockdown in endothelial cells reduces monocyte TEM. (A)** HUVECs were fixed, permeabilized, stained for IQGAP1 and PECAM, and visualized using widefield fluorescence microscopy. Merged panel shows IQGAP1 in green and PECAM in red. Yellow indicates colocalization. Scale bar represents 50 µm. **(B)** HUVECs were transduced with the indicated shRNAs against IQGAP1 or control shRNA (Cont; scrambled). 3 d after the transduction, the cells were lysed and their protein content resolved using SDS-PAGE and probed using Western blotting. Actin is shown as a loading control. MW, molecular weight. **(C)** HUVECs treated as in B. visualized using immunofluorescence as in A. Both images were collected under the same settings in the same experiment and processed identically. Scale bar represents 50 µm. **(D)** The transmigration of monocytes across HUVECs grown on collagen gels transduced with IQGAP1 shRNAs or control as detailed in B. The mouse anti-human PECAM antibody hec7 was included as a control. Data represent the average and standard deviation of three independent experiments, each of which was comprised of at least three samples and >100 leukocytes scored per sample for each condition. *, $P < 0.01$.

Results

IQGAP1 in the endothelial cell is required for TEM

We identified IQGAP1 in a screen for LBRC interacting proteins suggesting that it could play a role in the structure and/or function of the LBRC (Sullivan et al., 2014). To investigate this further, we examined the subcellular localization of IQGAP1 in primary endothelial cells (HUVECs) using immunofluorescence (Fig. 1 A). As shown previously, IQGAP1 is partially localized to the cytoplasm but is also prominent at endothelial cell–cell contacts along with PECAM (Nakhaei-Nejad et al., 2010; Sullivan et al., 2014; Tian et al., 2016). To examine IQGAP1 function in endothelial cells, we designed two knockdown shRNA constructs targeting its 3′ untranslated region (UTR; Table 1). Disruption of IQGAP1 expression using adenoviral transduction of these

Table 1. **Primers used in this study**

Primer name	Primer sequence (5′–3′)
IQGAP1 shRNA KD1 3′UTR nt649 forward[a]	ACCAGGAGTTACACAAACAGAATTGCCTTTTTTGAATTCTCGACCTCGAGACAAATGGCAG
IQGAP1 shRNA KD1 3′ UTR nt649 reverse[a]	ACCTGGAGTTACACAAACAGAATTGCCCCCGGTGTTTCGTCCTTTCCACAAGATATATAAAGC
IQGAP1 shRNA KD2 3′UTR nt576 forward[a]	ACCACTTCCTTTGAACATGACTGTCACTTTTTTGAATTCTCGACCTCGAGACAAATGGCAG
IQGAP1 shRNA KD2 3′ UTR nt576 reverse[a]	ACCTCTTCCTTTGAACATGACTGTCACCCCGGTGTTTCGTCCTTTCCACAAGATATATAAAGC
IQGAP1 mRNA amp forward	ATGTCCGCCGCAGACGA
IQGAP1 mRNA amp reverse	TTACTTCCCGTAGAACTTTTTGTT
IQGAP1 nt1 SalI Kozak forward	GCACGTCGACGCCACCATGTCCGCCGCAGACGA
IQGAP1 nt493 SalI Kozak forward	GCACGTCGACGCCACCATGGCCCCTCAGATTCAAGACCTATATG
IQGAP1 nt2190 XmaI reverse no stop	TCTCCCCGGGTGATAGAACTCTGGATCTCCTCCC
IQGAP1 nt2850 XmaI reverse no stop	TCTCCCCGGGACATCATCATAATATCAGACAACTGTTC
IQGAP1 nt4791 XmaI reverse no stop	TCAGCCCGGGACTTCCCGTAGAACTTTTTGTTG
IQGAP1 nt2188 Sal1 Kozak forward	GCACGTCGACGCCACCATGTCTGGGGTGACTGCCGCATATAACC
IQGAP1 nt2590 iqmot4 del forward[a]	CCTCCTATGGTTGTGGTCCGAAAATTTGTCC
IQGAP1 nt2253 iqmot1 del reverse[a]	CCTGGTGATCAGGCCTTCATTGGCC
PacI silent mutation forward[a]	GAGGATTTTAGCCATTGGTTTGATTAATGAAGCCCTGGATGAAG
PacI silent mutation reverse[a]	CTTCATCCAGGGCTTCATTAATCAAACCAATGGCTAAAATCCTC

[a]These primers also contained a 5′ phosphate.

constructs in primary endothelial cells (HUVECs) reduced IQGAP1 protein levels by ∼90% (Fig. 1 B). Interestingly, the residual IQGAP1 was still observed at both the junction and in the cytoplasm and appeared proportionately decreased from both (Fig. 1 C). We examined monocyte TEM using a standard TEM assay in which primary human peripheral blood mononuclear cells (PBMCs) are allowed to migrate across cytokine-activated endothelial cells grown on collagen matrices. This assay examines the behavior of monocytes. Lymphocytes do not migrate under these conditions (Muller and Weigl, 1992). 78 ± 2% of monocytes were able to transmigrate across endothelial cells transduced with scrambled shRNA (Fig. 1 D). However, when endothelial cells were transduced with IQGAP1 shRNA, TEM was reduced to 38 ± 4%, a level that is close to the blockade observed when PECAM homophilic interactions are disrupted with the mouse anti-human PECAM antibody hec7. The combination of anti-PECAM antibody and IQGAP1 knockdown was not additive (Fig. 1 D).

IQGAP1 is required for directing the LBRC to the site of TEM

We showed previously that during TEM the endothelial cell delivers membrane of the LBRC to the migrating leukocyte and that this targeted delivery (which we refer to as targeted recycling) is crucial to the process. Given the association of IQGAP1 with the LBRC, we wanted to examine the effect of knockdown of IQGAP1 expression on the structure and function of the LBRC. Immunochemical fractionation studies (Feng et al., 2015) demonstrated that the size of the LBRC was not changed in IQGAP1 knockdown cells (Fig. 2). We next performed the standard targeted recycling assay (Mamdouh et al., 2003, 2008, 2009; see Materials and methods) in which recycling LBRC membrane is detected as an enrichment of fluorescence (typically >2× that of adjacent uninvolved junction) around transmigrating leukocytes caught in the act of TEM (Fig. 3 A). Note that a "gap" of VE-cadherin expression is present at the site of TEM, as expected (Shaw et al., 2001), where targeted recycling of LBRC occurs (Gonzalez et al., 2016), as previously published. After allowing TEM to proceed for 10 min, the majority (∼90%) of adherent monocytes were found at endothelial cell borders in both control and IQGAP1 knockdown endothelial cells. On control endothelial cells, 31 ± 5% of adherent monocytes have extended pseudopods into the junction and have enriched fluorescence signal indicating targeted recycling of the LBRC (Fig. 3 B). By contrast, only 5 ± 3% of IQGAP1-depleted endothelial cells had increased LBRC fluorescence adjacent to infiltrating monocytes. (Note that virtually all monocytes in the act of TEM on control endothelial cells showed LBRC enrichment. Only ∼30% were in the act of TEM at the time the assay was stopped.) Because there was no effect on monocyte adhesion or their migration to the cell borders, these findings suggest that IQGAP1 plays an important role specifically in directing the LBRC to the site of TEM.

PECAM cross-linking recruits IQGAP1

We next wanted to examine the localization of IQGAP1 during TEM. PBMCs were allowed to migrate across endothelial cells for 10 min and then fixed to arrest them in the various stages of TEM. These samples were stained for IQGAP1 and examined using immunofluorescence microscopy to determine where endothelial cell IQGAP1 is localized during TEM (Fig. 4 A). In these assays, however, the intense IQGAP1 fluorescence detected in the migrating monocyte overshadowed that of endothelial IQGAP1, making it impossible to accurately determine if

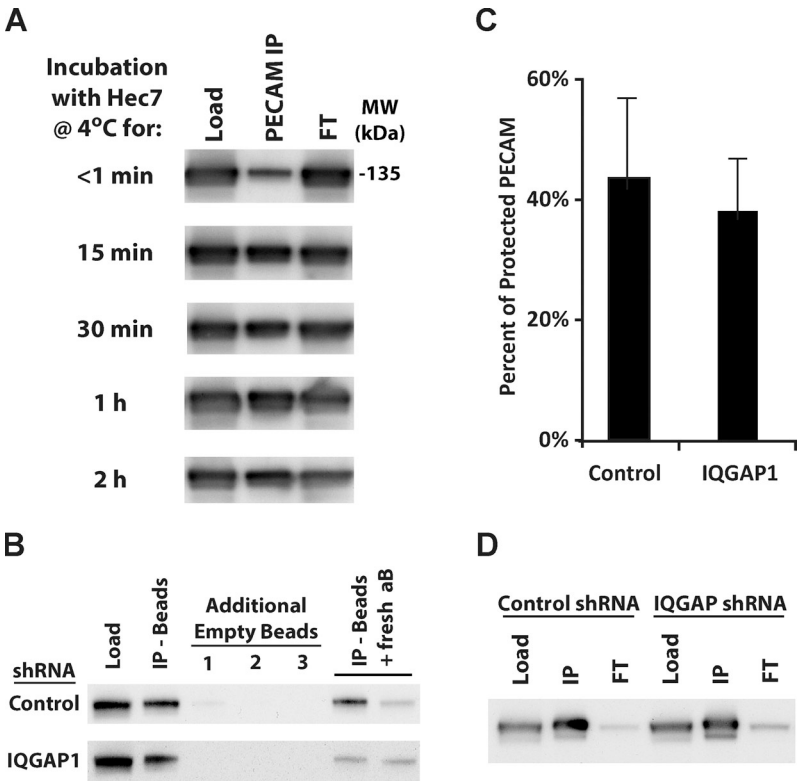

Figure 2. **The amount of PECAM protected in the LBRC at 4°C is not affected by IQGAP1 knockdown. (A)** HUVECs were chilled to 4°C and incubated with the monoclonal anti-PECAM antibody hec7 for the indicated time before being washed extensively and lysed. Lysates were incubated with recombinant Protein-G agarose beads to recover the surface PECAM that had been exposed and was bound to antibody (PECAM IP). PECAM that was not bound at 4°C (which had either not had time to bind PECAM or was protected in the LBRC) was recovered in the flow through (FT). The amount of PECAM in the various fractions was analyzed using Western blotting for PECAM (PECAM relative mobility, 135 kD; all blots in this figure are for PECAM). Equivalent amounts of each sample were loaded to allow for direct comparison of signal intensity for each time point (i.e., the amount of PECAM recovered in the immunoprecipitate (IP) corresponds directly to the amount reduced in the FT). The time course shows that the accessible surface pool of PECAM is quickly bound and saturated at 4°C. MW, molecular weight. **(B)** Control and IQGAP1 knockdown HUVECs were incubated with the anti-PECAM antibody hec7 at 4°C for 2 h as in A. After extensive washing and lysis, surface PECAM that was able to bind hec7 was recovered using Protein-G beads. To make sure the hec7-bound PECAM was fully recovered, the supernatant from the first IP was transferred to tubes with fresh Protein-G beads. This was repeated three total times (additional empty beads 1–3) before recovering the remaining LBRC-protected PECAM with additional Protein-G beads and hec7 (last lane, IP – beads + fresh antibody [aB]). The remaining FT was checked to make sure that all of the PECAM in the sample was recovered in the IPs (not shown). Equivalent amounts of each sample were loaded to allow for direct comparison of signal intensity. **(C)** The amount of PECAM recovered in each IP was quantified using densitometry. The amount that was protected from antibody at 4°C was calculated by dividing the amount recovered in the last IP by the total amount recovered in all IPs. Knockdown of IQGAP1 had no effect on the amount of PECAM that was protected at 4°C. The result was the same when calculated using the lysate (first lane) for the total amount of PECAM. Data shown are representative of three independent experiments, and error bars denote the standard deviation. **(D)** Because recently internalized (e.g., in endosomes) and intracellular (e.g., newly synthesized, but not yet trafficked to the surface) PECAM would be indistinguishable from LBRC-protected PECAM in the assays detailed in A–C, the amount of PECAM on the surface and the LBRC was examined for control and IQGAP1 knockdown HUVECs. Confluent monolayers were incubated for 15 min at 37°C with hec7 to label total plasma membrane PECAM (surface and LBRC). Cells were washed extensively to remove unbound antibody, lysed, and incubated with Protein-G beads to recover antibody-bound PECAM. The relatively small amount of PECAM left in the FT suggests that ablation of IQGAP1 does not alter the expression or intracellular distribution of PECAM.

endothelial cell IQGAP1 is recruited to the TEM pore. To examine this in another way, we incubated endothelial cells with anti-PECAM antibody–coated beads. When these beads settle on endothelial cells, they replicate some of the signals that a leukocyte would deliver by cross-linking and/or clustering some of the proteins involved in TEM and, in doing so, trigger the recruitment of downstream signaling molecules (van Buul et al., 2007; van Rijssel et al., 2012; Sullivan et al., 2013; Watson et al., 2015; Weber et al., 2015). Endothelial cells were incubated with beads coated with either nonspecific mouse IgG or anti-PECAM, anti-MHC class I, or anti-ICAM-1 antibodies and stained for IQGAP1. The signal intensity of the IQGAP1 fluorescence adjacent to the bead was then compared with the intensity in nearby regions. Only ∼20% of beads coated with nonspecific or anti-MHC class I antibody induced an increase of >1.5 fold in IQGAP1 fluorescence adjacent to sites of adhesion (Fig. 4, B and C). By contrast, endothelial IQGAP1 fluorescence was enriched at 66 ± 12% sites where anti-PECAM–coated beads adhered to cells. The IQGAP1 signal seen around anti-PECAM beads clearly extended beyond the region of contact with the bead, making it unlikely to be an optical artifact. Similar recruitment was seen with beads coated with antibodies against poliovirus receptor (data not shown), which functions immediately downstream of PECAM in TEM (Sullivan et al., 2013). As a positive control, we also examined IQGAP1 recruitment to anti-ICAM-1–coated beads. As expected, ICAM-1 engagement was able to recruit IQGAP1, which is likely due to the ICAM-1–meditated recruitment of EB1 and cortactin (Schnoor et al., 2011; Tian et al., 2014). Taken together with the previous findings, these data suggest that endothelial cell IQGAP1 is directed to the migrating leukocyte in a PECAM-dependent manner and, either directly or indirectly, recruits the LBRC.

The actin-binding domain of IQGAP1 is required for its junctional localization

IQGAP1 interacts with different classes of molecules through one of six defined domains (Fig. 5 A). To determine which domains of IQGAP1 are necessary and sufficient for its role in TEM, we designed a series of IQGAP1 truncation mutants for expression in control and IQGAP1-depleted cells. These constructs were engineered with a C-terminal GFP tag and designed to start and/or stop between adjacent well-characterized conserved IQGAP1 domains as previously identified (Briggs and Sacks, 2003b; Fig. 5 A and Tables 1 and 2). The subsequent in vitro experiments were

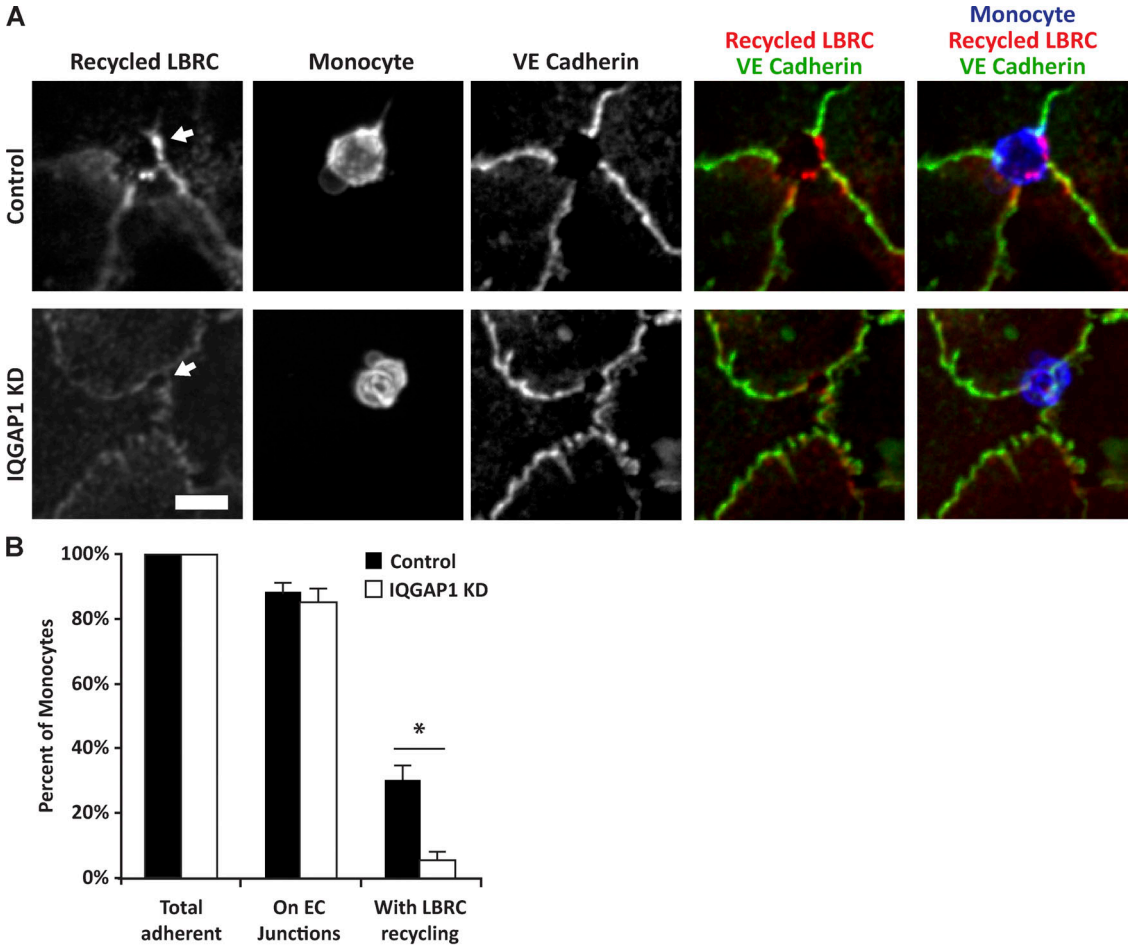

Figure 3. **IQGAP1 is required for the targeted recycling of the LBRC. (A)** HUVECs grown on collagen gels and transduced with control or shRNA against IQGAP1 (knockdown, KD) as in Fig. 1 were subjected to the targeted recycling assay (described in Materials and methods), which follows the directed movement of LRBC to the site of transmigration. When visualized using immunofluorescence microscopy, recycled LBRC is observed as increased fluorescence adjacent to monocytes (visualized with anti-CD18). Staining of the same monolayers for VE-cadherin shows the expected gap in fluorescence where TEM is proceeding (denoted by the arrows). Images shown were contrast adjusted identically and are representative of three independent experiments. **(B)** Quantification of the monocyte position and LBRC recruitment shown in A. Monocytes were considered to be on the endothelial cell (EC) junction if they overlapped at all with the junction. Data shown are the average and standard deviation of three independent experiments, with at least 50 monocytes scored per experiment. Data from each experiment were normalized to the total adherent cells to account for subtle differences in adhesion on each monolayer. Scale bar represents 20 µm. Note that this is a snapshot of a short time point, so only approximately one third of adherent monocytes on control monolayers are actively transmigrating at this time. *, $P < 0.01$.

performed using immortalized HUVECs (iHUVECs), which can be transduced more reproducibly than HUVECs. Whenever examined, iHUVECs behaved identically to primary HUVECs with regard to TEM and LBRC function (Yang et al., 2005; Sullivan et al., 2014; Feng et al., 2015; Watson et al., 2015). All truncation constructs were detected at their predicted apparent molecular weights (Fig. 5 B). Note that the IQGAP1 shRNA construct was designed against the 3′ UTR of IQGAP1 and only targets the endogenous IQGAP1. When examined using fluorescence microscopy, the full-length (FL) construct was observed partially localized to the junction and partially in the cytoplasm (Fig. 5 C), similar to the distribution of endogenous IQGAP1 (Fig. 1). As a control, we expressed GFP alone, which was observed in the cytoplasm and the nucleus. Only the GFP control was observed in the nucleus, perhaps because it is small enough to passively diffuse through the nuclear pore complex. Of the various IQGAP1 constructs, deletion of the IQ, GRD, and RasGAP C-terminal domains (constructs Δ5,6 and Δ4-6) did not noticeably change the localization or the amount of the construct colocalizing with PECAM (Fig. 5 C). Careful analysis and quantitation of the fluorescence intensity of PECAM, VE-cadherin, and the various constructs at the perijunctional region in a number of separate cells showed that PECAM and VE-cadherin distribution were largely unaffected by IQGAP1 knockdown and construct reexpression (Fig. 6). In addition, knockdown of IQGAP1 and reexpression of these constructs did not change the distribution of CD99, ICAM-1, actin filaments, or microtubules (Figs. S1, S2, S3, S4, and S5). However, constructs that lacked the N-terminal actin-binding CH domain (constructs Δ1 and Δ1,5,6), were not observed at the junction,

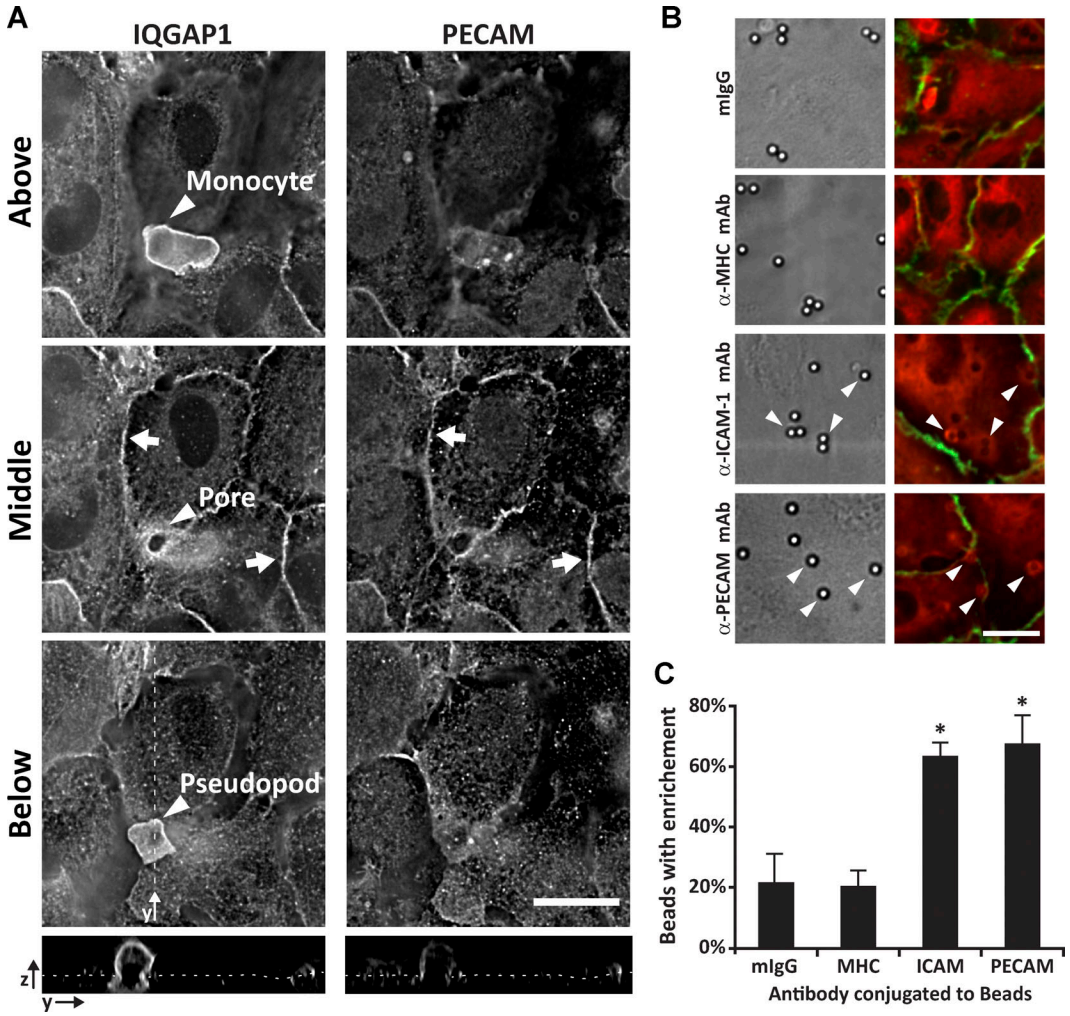

Figure 4. **IQGAP1 is recruited to anti-PECAM–coated beads. (A)** HUVECs were incubated with PBMCs for 10 min before being fixed, stained for IQGAP1 and PECAM, and visualized using immunofluorescence microscopy. Deconvolved images shown are slices from a z-series of a monocyte in the act of TEM and show the monocyte (arrowhead in each slice) cell body above the monolayer, in the middle of a transmigration pore, and its pseudopod below the monolayer. Arrows point to endothelial cell borders. Scale bar represents 25 µm. Bottom panels show the yz orthogonal view along the dashed line displayed in the "Below" panel. The thin dotted line indicates the surface of the endothelium. **(B)** HUVECs were incubated with beads coated with nonspecific mouse IgG (mIgG) or mouse anti-human MHC (α-MHC), ICAM-1 (α-ICAM-1), or PECAM (α-PECAM) antibodies for 20 min and then fixed, stained for IQGAP1 (red) and junctions (anti-VE-cadherin, green), and visualized using differential interference contrast (left column) and confocal immunofluorescence (right column). Arrowheads denote beads displaying IQGAP1 enrichment. Scale bar represents 25 µm. **(C)** Quantitation of the data shown in B. A bead was considered to have enriched IQGAP1 if the adjacent fluorescence signal was at least 1.5-fold higher than the nearby off-bead signal. Data shown are the average and standard deviation from three experiments, with >100 beads quantified per experiment per condition. *, $P < 0.05$ relative to mIgG control. Representative images are shown.

indicating that the CH domain is required for localization to the junctions.

The actin-binding domain and IQ motifs facilitate TEM

We next sought to determine which of these constructs could rescue the defect in TEM caused by the knockdown of endogenous IQGAP1. Monocytes were allowed to transmigrate across cytokine-activated control and IQGAP1 knockdown iHUVECs expressing the GFP-tagged truncation constructs after which the samples were fixed and TEM quantified. As with primary endothelial cells (Fig. 1 A), in control iHUVECs (control shRNA, reexpression construct encoding GFP alone), roughly 80% of the monocytes were able to undergo transmigration (Fig. 7 A). This is in contrast to IQGAP1-depleted cells (IQGAP1 shRNA, expressing GFP), which supported <40% TEM. This defect could be rescued entirely by the expression of the FL construct and the Δ5,6 construct, from which the GRD and RasGAP domains are deleted. However, constructs lacking either the actin-binding CH domain (constructs Δ1 and Δ1,5,6) or the IQ domain (construct Δ4-6) were unable to rescue TEM. Note, however, that they did not have a dominant negative function in cells containing endogenous IQGAP1 (black bars). The same requirements for domains 1 and 4 were found for TEM of neutrophils (Fig. 7 B). Since the CH domain was involved in targeting IQGAP1 to the junctions, this result indicates that there is an additional role for the IQ-motifs domain specifically in TEM.

To see if this was due, in part, to changes in the inherent function of the endothelial junctions in the transduced cells, we

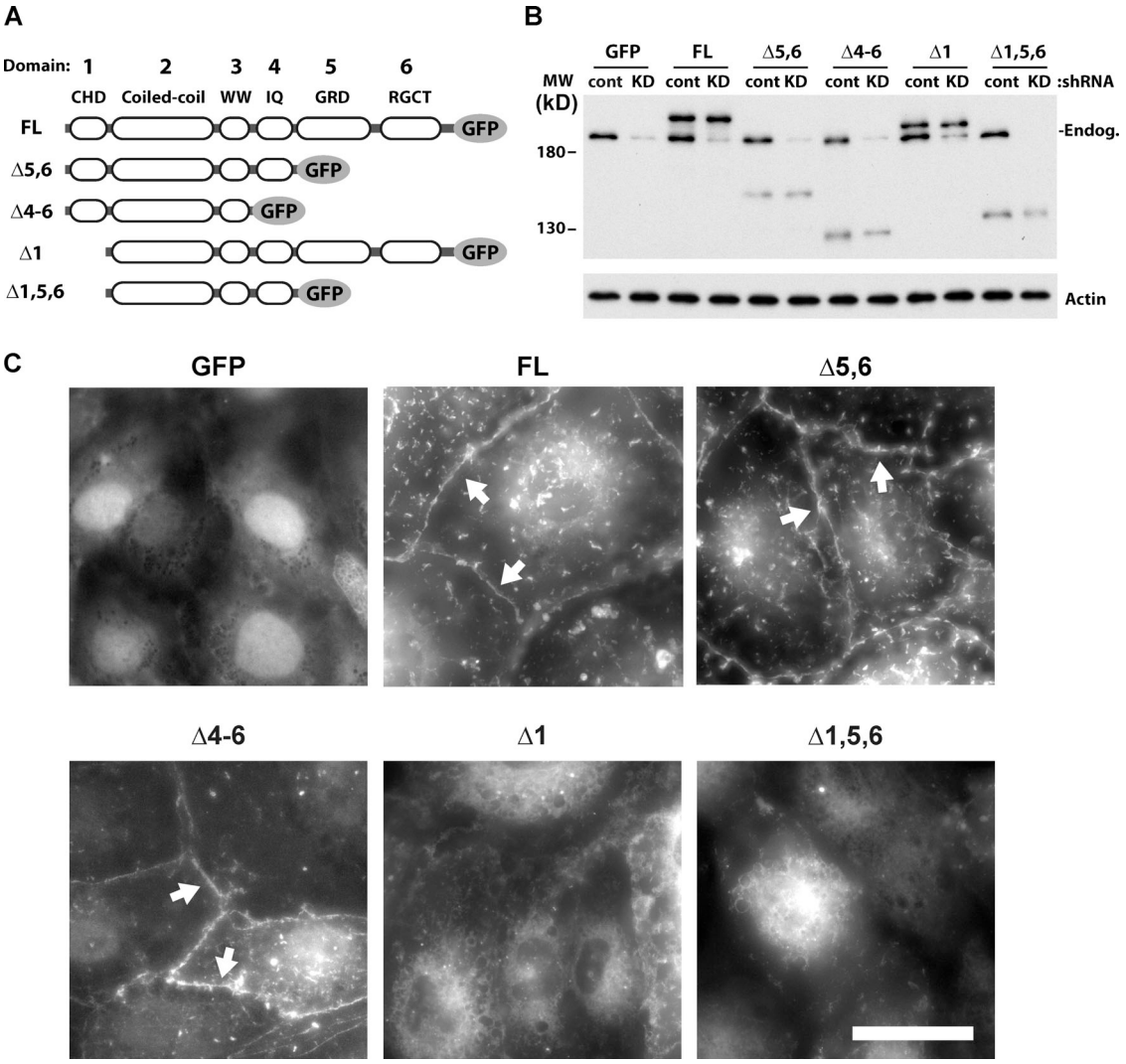

Figure 5. **The actin-binding domain of IQGAP1 is required for its localization to endothelial cell junctions. (A)** Schematic showing the naming of the various domains of IQGAP1 and the truncations used in this study. GRD, RasGAP-related domain; IQ, IQ motifs; RGCT, RasGAP C-terminus; WW, tandem tryptophan-containing domain. **(B)** The GFP-tagged constructs shown in A. were transduced into control (cont) or IQGAP1 shRNA (knockdown, KD) iHUVECs grown on collagen gels. After 2 d of reexpression of the truncation constructs (which corresponds to 3 d of transduction of the control/KD constructs), the cells were lysed and their protein content resolved with SDS-PAGE and probed using Western blotting. The blot shown has been probed for IQGAP1 using a polyclonal antibody against the coiled-coil domain, which is present in all constructs. Arrow denotes the relative mobility of endogenous IQGAP1. MW, molecular weight. **(C)** Immunofluorescence images of GFP IQGAP1 constructs transduced in iHUVECs as in B. The images shown were collected in the green channel using the same settings and processed identically. Arrows denote observed junctional localization of the indicated construct. The images shown are representative more than three independent experiments. Scale bar represents 50 µm.

subjected the various knockdown and rescue endothelial cells to a standard permeability assay (Winger et al., 2014). iHUVECs transduced as described above were incubated with low-molecular-weight rhodamine-dextran (10 kD) for 1 h in the presence of TNFα, after which the amount that passively diffused across the endothelial cells was quantified (Fig. 7 C). Compared with control, iHUVECs treated with the inflammatory stimulus TNFα were modestly more permeable. However, none of the constructs (knockdown, control, or truncation) had an appreciable effect either way on the permeability of the endothelial monolayers. These results suggest that domain 4 of IQGAP1 is required for its function in TEM. We also examined the vascular integrity in vivo; however, there was no detectable difference in vascular permeability between WT and IQGAP$^{-/-}$ animals as measured using the Miles assay (Schulte et al., 2011; Radu and Chernoff, 2013; Fig. 7 D).

The actin-binding domain and IQ motifs of IQGAP1 must be on the same molecule to facilitate TEM

Although the Δ4-6 construct is observed at the junction suggesting that the polypeptide is not substantially misformed, the inability of the Δ4-6 construct to rescue the knockdown of IQGAP1 could be due to misfolding of the protein fragment. To examine this possibility, we designed a construct with the internal deletion of domain 4 (construct Δ4), which lacks only the four IQ motifs and expressed it in IQGAP1 knockdown

Table 2. **Primer pairs used for generating the IQGAP1 truncation constructs**

Construct name	Forward primer	Reverse primer
FL	IQGAP1 nt1 SalI Kozak forward	IQGAP1 nt4791 XmaI reverse no stop
Δ5,6	IQGAP1 nt1 SalI Kozak forward	IQGAP1 nt2850 XmaI reverse no stop
Δ4-6	IQGAP1 nt1 SalI Kozak forward	IQGAP1 nt2190 XmaI reverse no stop
Δ1	IQGAP1 nt493 SalI Kozak forward	IQGAP1 nt4791 XmaI reverse no stop
Δ1,5,6	IQGAP1 nt493 SalI Kozak forward	IQGAP1 nt2850 XmaI reverse no stop
Δ1-3	IQGAP1 nt2188 Sal1 Kozak forward	IQGAP1 nt4791 XmaI reverse no stop
Δ4	IQGAP1 nt2590 iqmot4 del forward	IQGAP1 nt2253 iqmot1 del reverse

endothelial cells (Fig. 8, A and B). This construct had the same junctional and cytoplasmic distribution as endogenous and the FL IQGAP1-GFP construct (compare Fig. 8 C to Figs. 5 C and 1 A) suggesting that the construct was expressed and properly localized. However, it was unable to rescue the TEM of monocytes on IQGAP1 knockdown cells (Fig. 8 D), further confirming the requirement of the IQ domain for IQGAP1's function in TEM.

Homodimerization of IQGAP1 has been reported to be important for its function (Bashour et al., 1997; Fukata et al., 1997; Mateer et al., 2002), which has implications for its mechanism of action. For example, oligomerization of IQGAP1 has been shown to be necessary for increasing activation of Cdc42 (Ren et al., 2005). Therefore, we examined whether the localization and function of IQGAP1 in TEM required domains 1 and 4 to be on the same monomer. Additional truncation constructs were made as before but with mCherry instead of GFP, which allowed for identification of the various constructs when coexpressed with the corresponding GFP constructs and visualized using immunofluorescence. These constructs were transduced in IQGAP1 knockdown endothelial cells along with the indicated GFP constructs (Fig. 8 B). None of the constructs had a dominant-negative effect, as no disruption of TEM or endogenous IQGAP1 localization was observed (data not shown) in control (no knockdown) monolayers. As before, constructs that contained domain 1 were observed at least partially at endothelial cell junctions, whereas those without (construct Δ1-3-mCherry and Δ1-GFP) did not colocalize with VE-cadherin at the junction (Fig. 8 C). Interestingly, neither the coexpression of Δ1-GFP with Δ4-6-mCherry (which both contain domains 2 and 3) nor Δ4-6-GFP with Δ1-3-mCherry (which contain no overlapping domains) was able to rescue the TEM defect caused by IQGAP1 knockdown. Furthermore, in both combinations, constructs that contained domain 1 were unable to recruit the corresponding construct lacking domain 1 to the junction. Together, these findings show that IQGAP1's function in TEM requires domains 1 and 4 to be on the same molecule.

IQGAP1 is required for TEM in vivo

We next wanted to extend these studies in vivo but reasoned the results collected using whole-animal IQGAP1 knockout could be confounded by the potential function of IQGAP1 in leukocytes. To simplify the interpretation of these studies, since a conditional IQGAP1 knockout mouse does not exist, we used adoptive bone marrow transfer to make chimeras of WT donors and WT or IQGAP1$^{-/-}$ recipients so that all myelomonocytic cells and their derivatives would be WT, but in the knockout recipients, the endothelial cells (and other tissues) would lack IQGAP1 expression. We first examined TEM using the croton oil dermatitis model of inflammation. For this assay, croton oil, a potent inflammatory stimulus, or carrier alone, was topically applied to both leaflets of one ear. After 5 h (to allow for sufficient recruitment of neutrophils), the animals were sacrificed and their ears harvested and processed for whole-mount confocal microscopy (Watson et al., 2015; Weber et al., 2015; Sullivan et al., 2016). Both chimeras recruited a similar number of neutrophils to the inflamed tissue. In WT recipients, the majority of these neutrophils were observed outside of blood vessels in the inflamed tissue (Fig. 9 A). In contrast, neutrophils in the IQGAP1$^{-/-}$ recipients were mostly still inside the venules. Furthermore, we used confocal microscopy to distinguish the precise position of the recruited neutrophils relative to the endothelium and basement membrane, which we assigned according to a standard scoring method (Fig. 9 B). We systematically scored the neutrophil positions in at least five fields from five WT and 6 IQGAP1$^{-/-}$ recipients. Although there was no difference in the total neutrophil recruitment to the inflamed ears between the two chimeras (Fig. 9 C), IQGAP1$^{-/-}$ recipients showed a significant reduction in the number of neutrophils observed outside the vessel with corresponding increase in the number observed with a portion of their cell body in the endothelium ("In TEM"; Fig. 9 D).

Although these findings support a role for IQGAP1 in TEM in vivo, we wanted confirmation using a second model that also allowed us to examine the process in live animals. To do this, we again used bone marrow chimeras as before, except that in these experiments, the donors expressed GFP under the control of the LysM promoter, which allows for the visualization of neutrophils using fluorescence intravital microscopy (IVM). These mice were injected intrascrotally with mouse IL-1β to induce inflammation and fluorescently conjugated nonblocking anti-PECAM antibody to label the vasculature in red to distinguish it from the green neutrophils (Sullivan et al., 2016). After 4 h, which allows for a robust inflammatory response, the cremaster muscle was exteriorized and visualized (Fig. 10 A and Videos 1 and 2). In both WT and IQGAP1$^{-/-}$ recipients, we observed similar (and typical) rates of neutrophil rolling flux (Fig. 10 B) and adhesion (Fig. 10 C; Sullivan et al., 2016). Purified human neutrophils crawling on either WT or IQGAP1$^{-/-}$ endothelium spent 90–95% of their time associated with a junction (not shown). However, in IQGAP1$^{-/-}$ recipients, there was a ∼80% reduction in TEM events compared with WT recipients (Fig. 10 D; 6 ± 4 events per 300 µm per hour compared to 42 ± 4 events, respectively).

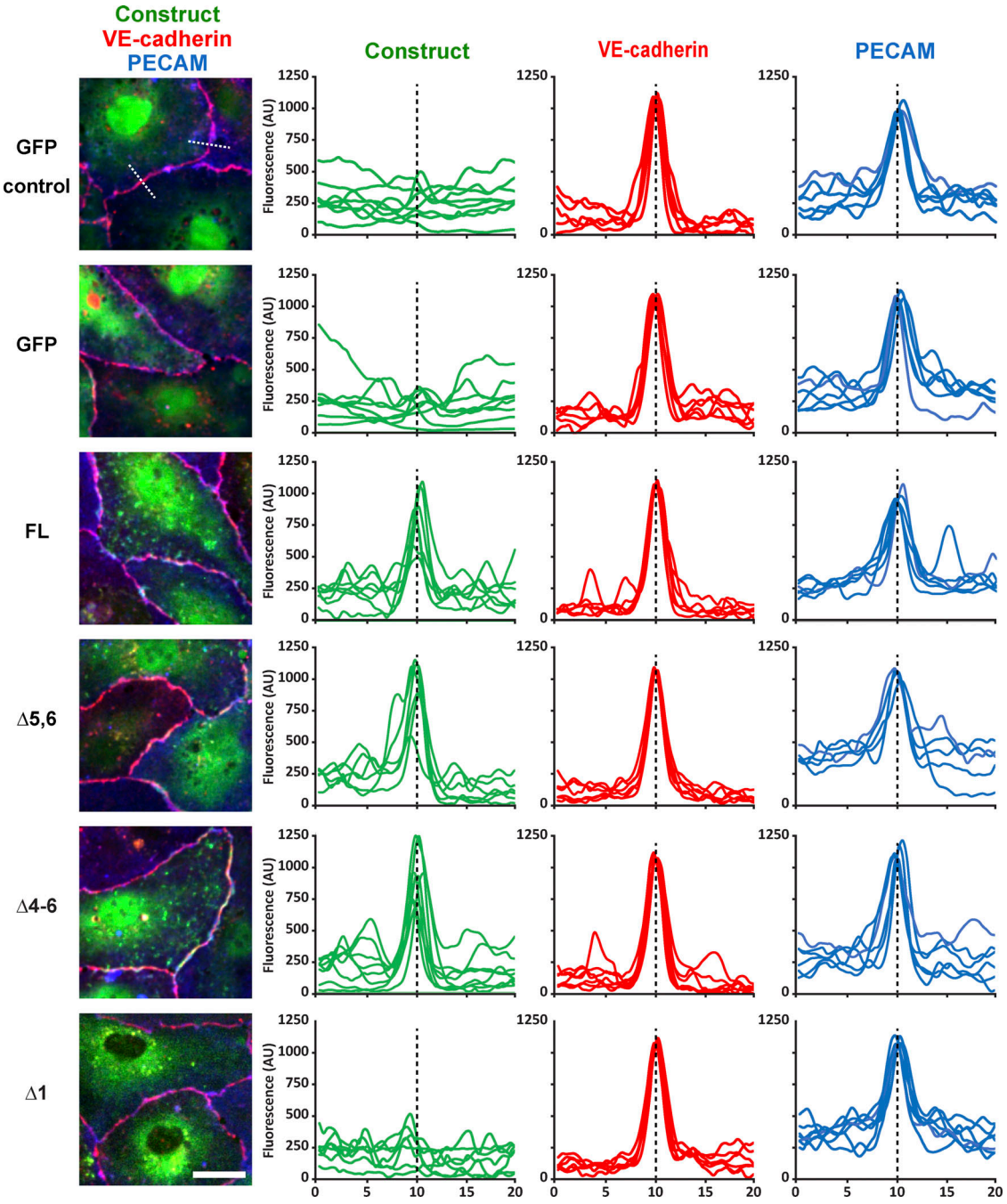

Figure 6. **Quantitation of the junctional localization of the IQGAP1 constructs.** iHUVECs were transduced with control shRNA (top row) or knockdown shRNA (other rows) and the indicated expression constructs as described in Materials and methods and confirmed in Fig. 7. Immunofluorescence images of PECAM, VE-cadherin, and the indicated IQGAP1 construct were analyzed for the enrichment of each molecule at the junction as described in Materials and methods. The left column (also shown in Fig. S1) shows a representative image for each of the constructs analyzed. For each junctional analysis, a 20-µm line was drawn centered on and perpendicular to the junction and the pixel intensity (normalized fluorescence, arbitrary units [AU]) along that line plotted as a histogram for each of channel separately. The compiled histograms collected from at least three different images and at least two random junctions are shown in the three right columns for the indicated GFP construct, VE-cadherin, and PECAM, respectively. Although the images were all collected under the same settings, the individual lines still needed to be adjusted relative to the each other to account for variations in staining intensity (for PECAM and VE-cadherin) and expression (for the IQGAP1 constructs). Note that this makes the intensities for the construct-GFP plots similar at the distal 0 µm and/or 20 µm ends of the plot but retains any meaningful differences at the junction in the middle. Only constructs that contained domain 1 (IQGAP1 FL; Δ5,6; and Δ4-6) were significantly enriched at the junction. Dashed white line in the top left panel shows two representative 20-µm lines that were analyzed. Dashed black line in each compiled histogram shows the midpoint of the 20-µm line plot, which corresponds to the center point of the junction. Scale bar represents 25 µm.

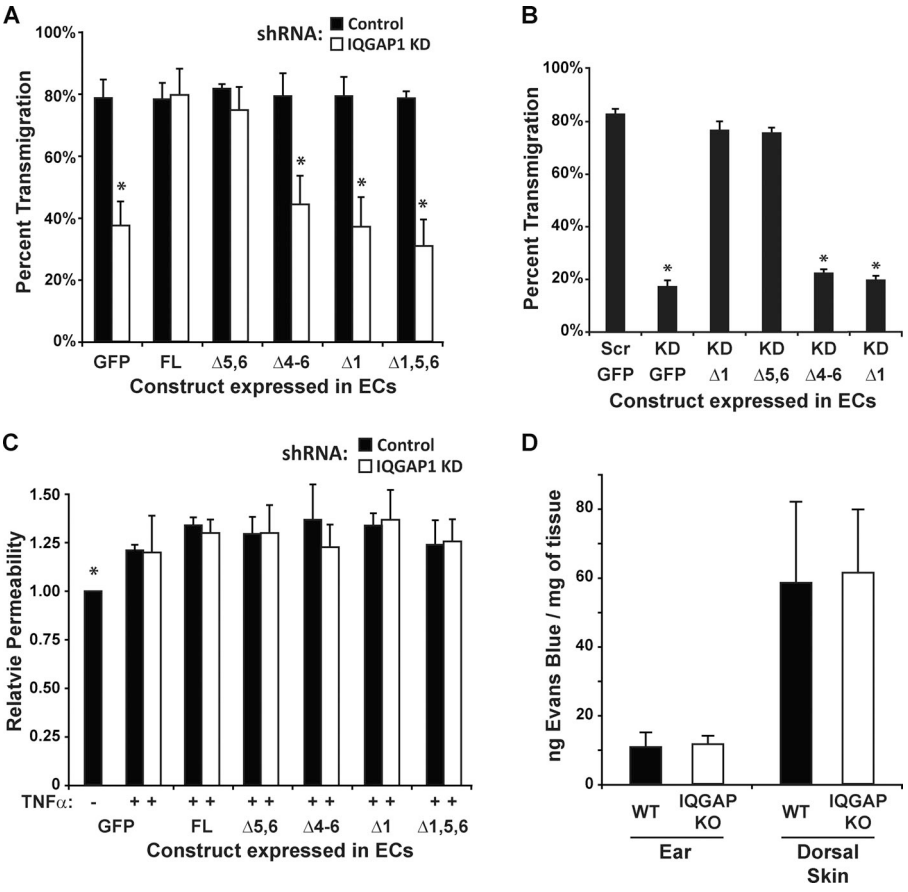

Figure 7. **The actin-binding domain and IQ motifs of IQGAP1 are required for IQGAP1's function in TEM. (A)** iHUVECs grown on collagen gels, transduced with the indicated control, knockdown (KD), and reexpression constructs, and stimulated with TNFα were incubated with PBMCs for 1 h, after which the samples were washed, fixed, stained, and visualized using bright-field microscopy as described in Materials and methods. Data shown represent the percentage of monocytes that were found beneath the endothelial cell (EC) monolayer and are the average and standard deviation from three experiments, each of which comprised triplicate samples for each condition. *, $P < 0.01$ compared with the knockdown-FL rescue control. **(B)** The same experiment as in part A was performed using purified human neutrophils. Transmigration was allowed to proceed for 15 min. **(C)** iHUVEC grown on collagen gels, transduced, and stimulated as described above. 2 d after the transduction of the truncation constructs, the monolayers were treated with rhodamine-dextran (molecular weight, 10 kD) for 1 h. After four quick washes, the fluorescence that had passed through the monolayer into the collagen gel was quantified using a fluorescence plate reader. Data were collected for each sample and normalized to the average observed with the GFP control shRNA samples within each experiment. Data shown for A–C are the average and standard deviation from three independent experiments, each of which contains triplicate samples for each condition. None of the conditions were statistically different ($P < 0.05$) from any other. **(D)** The Miles assay, measuring the vascular leakage of Evans Blue, was performed on the ears and dorsal skin of WT and IQGAP1 knockout mice. No statistical difference was observed between the two groups. Data shown are for four mice for each group.

Discussion

IQGAP1 is a scaffolding molecule that coordinates the interactions of >100 proteins involved in dozens of intracellular events involving the actin and microtubule cytoskeletons, cell polarity, cell adhesion, organelle trafficking, and cell signaling. In light of this, it may not come as a surprise that IQGAP1 has a role in TEM. However, considering the multiple and complex adhesive interactions, signaling pathways, membrane movements, and cytoskeletal rearrangements that are involved in the process of TEM, it is surprising to find a single IQGAP1-dependent mechanism that dominates the process; knockdown of IQGAP1 significantly reduced targeted recycling of the LBRC and therefore TEM, and both could be restored to control levels by expression of FL IQGAP1 or a version containing the CH and IQ domains. There was no effect on the size of the LBRC (Fig. 2), leukocyte adhesion or locomotion on the endothelial surface (Fig. 3), endothelial cell permeability (Fig. 7), or distribution of VE-cadherin (Fig. 6), PECAM, CD99, ICAM-1, microtubules, or actin filaments (Figs. S1, S2, S3, S4, and S5). We cannot rule out that there may be other IQGAP1-dependent processes ongoing in the endothelial cell that contribute to TEM. However, those processes would also have to require the CH and IQ domains to be present on the same molecule.

The data presented here provide the first demonstration that IQGAP1 is required for the TEM of monocytes and neutrophils, and, most importantly, show that IQGAP1 is selectively required for the diapedesis step of inflammation in vivo. There was no effect on leukocyte rolling flux, adhesion, or neutrophil crawling time (Fig. 10 and Videos 1 and 2). This was a true block in TEM, not merely a delay. Leukocytes remained blocked for the entire observation period; in contrast, control leukocytes completed TEM in a few minutes. Furthermore, we show the mechanism behind this: IQGAP1 is required for efficient delivery of the LBRC to migrating monocytes. Targeted recycling was significantly attenuated in IQGAP1 knockdown endothelial cells. As with other molecules selectively involved in the diapedesis step (Schenkel et al., 2002; Dasgupta et al., 2009; Mamdouh et al., 2009; Cyrus and Muller, 2016), leukocytes show no defect in their ability to bind to endothelial cells lacking IQGAP1 or their ability to migrate to cell junctions either in vitro or in vivo. In this regard, IQGAP1 is required for efficient TEM but does not activate it or appear to control a rate-limiting step. Expression of

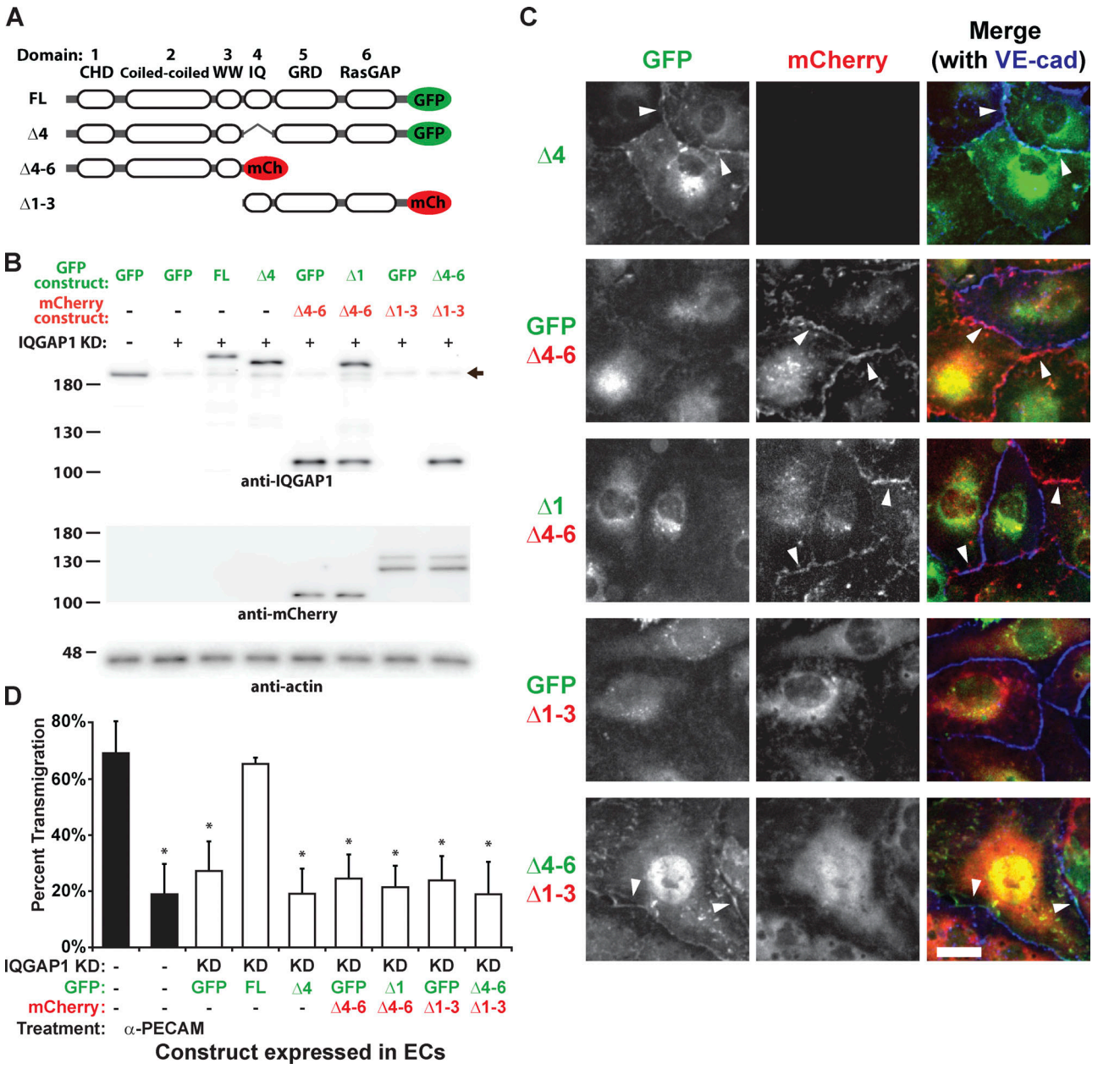

Figure 8. **The actin-binding domain and IQ motifs of IQGAP1 must be on the same molecule for IQGAP1 to function. (A)** Schematic showing the naming of additional IQGAP1 truncation constructs fused to GFP or mCherry. **(B)** The tagged constructs shown in A were transduced into control or IQGAP1 shRNA (KD) iHUVECs grown on collagen gels as indicated ("GFP" denotes monolayers expressing GFP alone). After 2 d of reexpression of the truncation constructs (which corresponds to 3 d of transduction of the control/KD constructs), the cells were lysed and their proteins resolved with SDS-PAGE and probed using Western blotting. The representative Western blots shown were probed for IQGAP1, mCherry, and actin using the indicated antibodies. Blots shown are from different gels/transfers of the same samples. Note that mCherry construct IQGAP1Δ1-3 (Δ1-3 in red) is not detected with the IQGAP1 antibody because it lacks the coiled-coil domain that is recognized by the antibody. Arrow denotes the relative mobility of endogenous IQGAP1. **(C)** Immunofluorescence images of the mCherry and GFP IQGAP1 constructs transduced in iHUVECs as in B. For each channel, the images shown were collected with the same settings and processed identically to preserve relative intensity differences. Arrowheads denote observed junctional localization of the indicated construct. The images shown are representative of more than three independent experiments. Scale bar represents 25 µm. **(D)** iHUVECs grown on collagen gels were transduced with the indicated constructs and subjected to the standard TEM assay (as described in Fig. 7 and the Materials and methods). The percent TEM is shown for the indicated IQGAP1 KD coexpression combinations along with control samples (black bars); no-knockdown expressing GFP alone and no-knockdown but TEM blocked with the function-blocking anti-PECAM antibody hec7 (α-PECAM). Data shown are the average and standard deviation from three experiments, each of which comprised triplicate samples for each condition. *, $P < 0.01$ compared with the knockdown-FL rescue control.

FL IQGAP1 or constructs containing the "minimal motif" in endothelial cells that already contain endogenous IQGAP1 do not increase the rate or extent of TEM (Fig. 7 A). Furthermore, constructs lacking domain 1 or 4 do not act as dominant negatives when expressed in endothelial cells with a normal complement of IQGAP1 (Fig. 7 A).

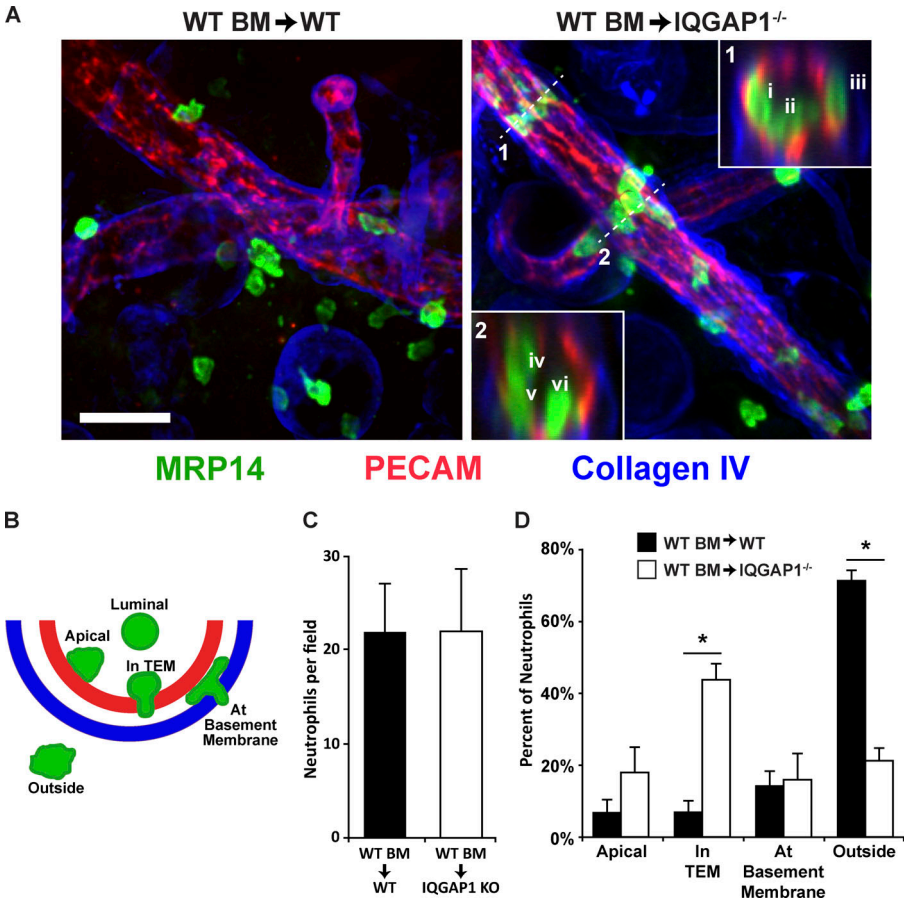

Figure 9. **IQGAP1 is required for neutrophil TEM in vivo. (A)** IQGAP1 knockout and WT mice were lethally irradiated and their bone marrow reconstituted from WT donors as described in Materials and methods. After allowing reconstitution of the mice, one ear of each mouse was treated topically with croton oil in an acetone/olive oil carrier while the other ear received the carrier only. After 5 h, the mice were sacrificed and their ears processed for immunofluorescence imaging using confocal microscopy. Representative images from WT (WT BM → WT) and IQGAP1 knockout (WT BM → IQGAP1$^{-/-}$) are shown. Neutrophils were visualized with an antibody against MRP14 (green), the vessel and junctions were detected using anti-PECAM, and the basement membrane was visualized using anti-Collagen IV. Insets show the orthogonal view at position denoted by the dashed line. Orthogonal inset 1 shows one leukocyte in TEM (i), one apical (ii), and one at the basement membrane (iii). Orthogonal inset 2 shows one leukocyte on the apical surface (iv) and two that are in TEM (v and vi). Scale bar represents 50 µm. **(B)** Schematic of the positional scoring system used to quantify the neutrophil locations observed in A. **(C)** Quantitation of the total number of neutrophils per field. Only neutrophils within 50 µm of the vessel were scored. **(D)** Quantitation of the leukocyte positions from the images collected in A. Data shown were collected from two separate experiments, each of which contained at least two mice per condition. At least five fields (corresponding to ≥100 neutrophils) for each mouse were analyzed (n = 5 for WT recipients and n = 6 for the IQGAP1$^{-/-}$ recipients). Data shown are the average of the averages for each mouse and do not include data for the neutrophils found in the luminal position. *, P < 0.01. Carrier-only ears showed no signs of inflammation; neutrophils were rarely found in the tissue or associated with vessels (data not shown).

Although IQGAP1 is partially localized to the cell borders and can interact with both actin filaments and microtubules, the role of IQAGP1 in TEM does not appear to be related to effects on junctional integrity. We found no effect of IQGAP1 knockdown on endothelial cell monolayer permeability in vitro (Fig. 7 C) or in vivo in IQGAP1 knockout animals (Fig. 7 D). It is now quite evident that leukocyte TEM and monolayer permeability are molecularly distinct phenomena (Schnoor et al., 2011; Wessel et al., 2014; reviewed in Vestweber et al., 2014; Muller, 2016a).

We originally identified IQGAP1 as a molecule enriched in isolated LBRC membrane fractions (Sullivan et al., 2014). However, we have not been able to coimmunoprecipitate IQGAP1 along with PECAM, suggesting that although both are critical for initiating TEM, their strong interaction is not required. Similarly, LBRC is trafficked along microtubules toward the plus end during TEM; however, we could not coimmunoprecipitate IQGAP1 with the microtubule plus-end–binding protein EB1 (not shown), and the function of IQGAP1 in TEM does not require the microtubule-interacting RasGAP C-terminal domain (Figs. 7 and 8). Furthermore, knockdown of IQGAP1 does not affect the expression or distribution of PECAM, VE-cadherin, CD99, ICAM-1, actin, or microtubules (Figs. 6, S1, S2, S3, S4, and S5).

The results reported here substantially extend our understanding of the role of IQGAP1 in TEM, which was previously observed in only a single in vitro model using lymphocytes (Nakhaei-Nejad et al., 2010). In that report, knockdown of IQGAP1 in HUVECs by siRNA was associated with a modest (30%) decrease in transmigration of lymphocytes (Nakhaei-Nejad et al., 2010) without a change in lymphocyte adhesion or migration to junctions, similar to what we found. As we had originally reported (Mamdouh et al., 2008), they also found that disruption of microtubules under conditions that did not perturb actin assembly or disrupt adherens junctions also inhibited TEM (Nakhaei-Nejad et al., 2010). Since IQGAP1 had been shown to interact with microtubules, and since siRNA inhibition of IQGAP1 and dissolution of microtubules produced the same phenotype, these authors concluded that the effect of IQGAP1 knockdown on TEM involved microtubule dynamics. However, that conclusion turned out to be incorrect. Intact microtubules are indeed required for TEM. They serve as tracks on which the LBRC moves (Mamdouh et al., 2008; Cyrus and Muller, 2016). In fact, knowing the critical role of microtubules in movement of the LBRC and the known interactions of IQGAP1 with microtubules, we at first thought that the role of IQGAP1 in targeted recycling of the LBRC would involve interactions with microtubules. We set out to test this hypothesis by rescuing IQGAP1 expression with IQGAP1 molecules missing established interaction domains. However, we found that although microtubules

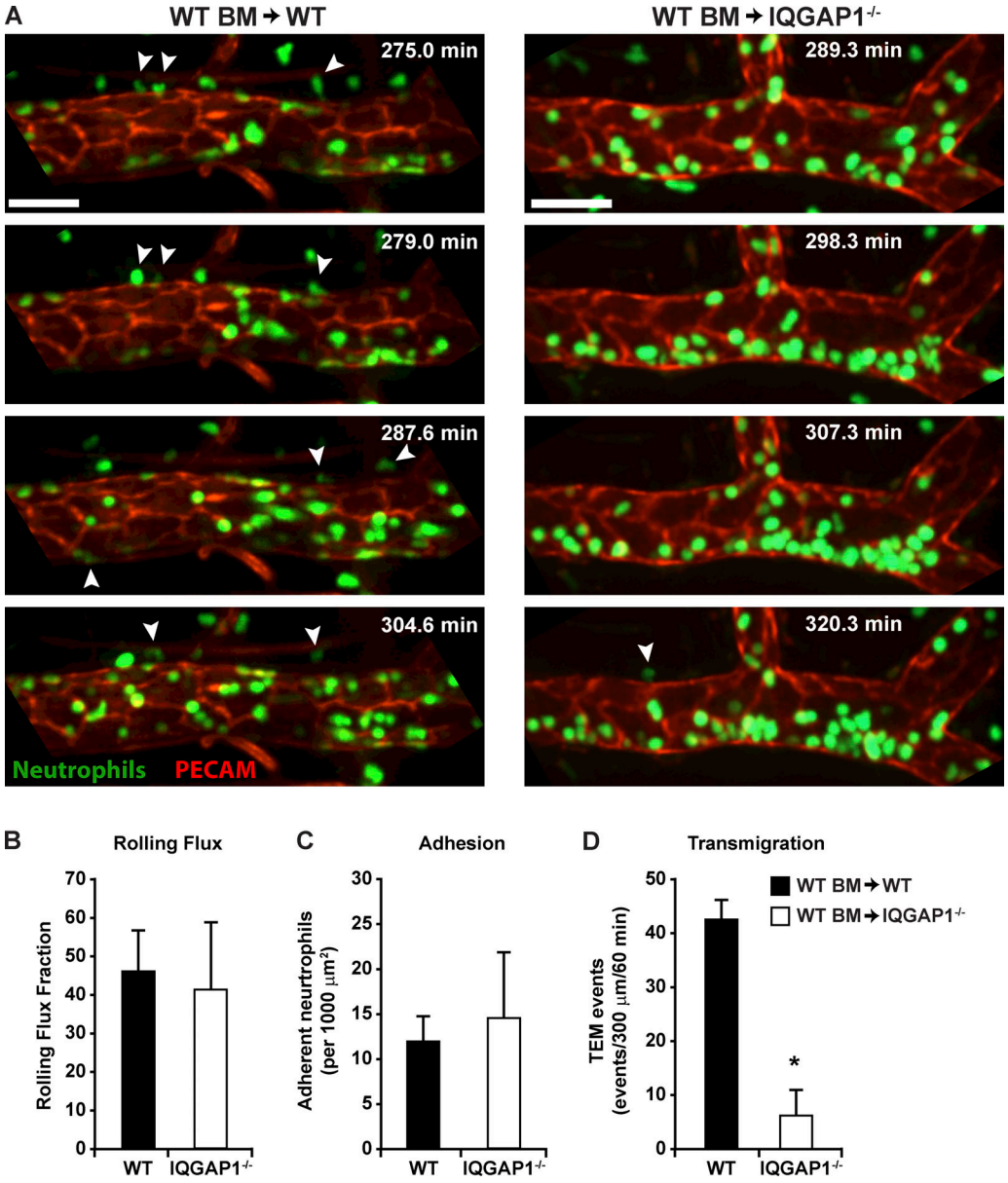

Figure 10. **IVM confirms a role for endothelial IQGAP1 in neutrophil TEM. (A)** WT and IQGAP1 knockout mice were reconstituted with bone marrow from mice expressing GFP under the control of the LysM promoter (for visualization of GFP^{hi} neutrophils). Inflammation was induced by intrascrotal injection of IL-1β. Nonblocking fluorescently conjugated anti-PECAM (red) was coinjected with IL-1β to allow for visualization of the vasculature. 4 h after the injection, the cremaster muscle was exteriorized and prepared for confocal microscopy as described in Materials and methods. The images shown are Z-projections of the 3D stacks collected at the indicated time points. The corresponding FL videos are in the supplemental materials. Time stamp denotes total elapsed time from the injection of inflammatory stimulus. Arrowheads denote neutrophils that are in the process or have recently undergone TEM. Scale bars represent 50 µm. **(B and C)** Quantification of the rolling flux and adhesion, respectively, of neutrophils as determined from the initial recording; the two groups of mice were not statistically different for these measurements. **(D)** Quantification of the number of TEM events observed during the longer recording. *, $P < 0.01$. Error bars denote standard deviation.

are clearly necessary for targeted movement of the LBRC in TEM (Mamdouh et al., 2008; Cyrus and Muller, 2016), the RasGAP C-terminal domain of IQGAP1 that interacts with microtubules is not required for its role in this process (Figs. 7 and 8). Furthermore, knockdown of IQGAP1 has no effect on the distribution of microtubules in the cell (Fig. S5).

Because IQGAP1 is a multidomain protein with >100 reported interacting partners, in order to begin to understand its role in TEM, we wanted to determine which of its domains are involved in this function. Using domain truncations, we show that both the N-terminal CH domain and the IQ domain are required for TEM (Fig. 7). Furthermore, we show that both the CH and the IQ domains are required to be on the same IQGAP1 molecule to support TEM. This suggests that even if the two domains (on separate polypeptide chains) are brought together via homodimerization, IQGAP1's function in TEM still cannot be restored. Alternatively, domains 1 or 4 could themselves be required for dimerization. To our knowledge, this is not only the first report

of a function for IQGAP1 that requires both the CH and IQ domains but also the first report that describes the requirement for two domains of IQGAP1 to be present in the same polypeptide chain. Numerous proteins have been shown in other systems to interact with domains 1 and 4 in other cell types and systems. Which of these possible interacting factors, if any, plays a role in TEM remains an area for future investigation.

The major interaction reported to be facilitated by the CH domain is with filamentous actin (reviewed in Nussinov and Jang, 2014; Abel et al., 2015; Watanabe et al., 2015). Our findings show that the CH domain is involved in targeting IQGAP1 to the cell cortex (Figs. 5 and 6). This localization in itself may be required for IQGAP1's function; i.e., without its CH domain, IQGAP1 may not be at the correct place to perform its essential function. Alternatively, IQGAP1 binding to actin may be part of its function in TEM. Indeed, the actin-bundling protein cortactin and other actin-binding proteins have been shown to regulate leukocyte TEM (Schnoor et al., 2011; Schnoor, 2015), and endothelial cell IQGAP1 has, in other systems, been shown to interact with cortactin (Usatyuk et al., 2009; Tian et al., 2014).

A putative role for the IQ motifs in TEM is more difficult to deduce, largely because this region has been shown to facilitate interactions with multiple proteins including myosin essential light chain, S100B, and calmodulin (Joyal et al., 1997; Weissbach et al., 1998; Pathmanathan et al., 2008; Malarkannan et al., 2012). IQGAP1 has four IQ motifs, each of which largely, although not exactly, conforms to the consensus sequence IQXXXRGXXXR (Bähler and Rhoads, 2002; Caride et al., 2010). Multiple reports indicate that the IQ motifs can bind apocalmodulin and Ca^{2+}/calmodulin, albeit with varying specificity (Mateer et al., 2002; Li and Sacks, 2003; Jang et al., 2011).

We and others have shown that calcium signaling is required for TEM (Huang et al., 1993; Su et al., 2000; Weber et al., 2015). The increase in intracellular free calcium triggered early in TEM occurs specifically through endothelial PECAM stimulating the activation of the divalent cation channel TRPC6 (Weber et al., 2015), although the downstream players in this pathway remain unknown. Ca^{2+}/CaM binding to IQGAP1 reduces binding of most of the IQGAP1 binding partners that have been examined, such as Cdc42, actin, and E-cadherin (Joyal et al., 1997; Li et al., 1999; Mateer et al., 2002). IQGAP1 is displaced from regions of cell–cell contacts upon global calcium influx (Mateer et al., 2002). Several reports show that IQGAP1 does not bind actin and Ca^{2+}/calmodulin simultaneously (Pelikan-Conchaudron et al., 2011; Liu et al., 2016). Targeted recycling is an iterative process (Watson et al., 2015). Perhaps IQGAP1 facilitates TEM by binding cortical actin and apocalmodulin in a steady state, primed for action. After an increase in local calcium concentration, the interaction between IQGAP1 and Ca^{2+}/calmodulin changes and IQGAP1 disassociates from actin, which could then undergo remodeling based on other local cues (Briggs and Sacks, 2003a), while the LBRC is freed to undergo another round to targeted recycling in a Ca^{2+}-dependent manner. This model remains to be tested. Clearly, further work will be required to determine which of these possible interactions (or others) mediate the function of IQGAP1 in TEM.

Materials and methods

Antibodies and proteins

Mouse anti-human PECAM IgG_{2a} (clone hec7; Muller et al., 1989), mouse anti-human CD99 IgG_1 (clone hec2; Schenkel et al., 2002), mouse anti-human VE-cadherin IgG_{2a} (clone hec1; Ali et al., 1997), Armenian hamster anti-mouse PECAM (clone 2H8; Schenkel et al., 2004), anti-ICAM-1 mAb (clone R6.5, hybridoma obtained from the American Type Culture Collection), mouse IgG2a anti–human MHC I (clone W6/32; Muller et al., 1989), mouse anti-human ICAM-1 (clone R6.5; Mamdouh et al., 2009), and mouse anti-human CD18 (clone IB4; Wright et al., 1983) were produced in the laboratory via hybridoma methodologies (Bogen et al., 1994; Ali et al., 1997). The nonfunction blocking mouse anti-human PECAM antibody (clone P1.1; Liao et al., 1997) was purified from ascites generously gifted from Peter Newman (Blood Center of Wisconsin, Milwaukee, WI) and digested to F(ab) (fragment antigen binding) fragments according to standard methods. Rabbit polyclonal anti-human PECAM (177) was produced as previously described (Muller et al., 1993). Mouse anti-human β actin (for Western blotting) and mouse anti-human tubulin (catalog number T6074) were purchased from Millipore Sigma (catalog number A2228, clone AC-74). Rabbit anti-mouse collagen IV (ab19808), phalloidin-iFluor 555 (ab176756, for visualizing actin with immunofluorescence microscopy), and rat anti-mouse myeloid-related protein 14 (MRP14; ab105472, clone 2B10) were purchased from Abcam. Rat anti-mouse PECAM (clone 390) was purchased from EMD Millipore. Rabbit anti-human IQGAP1 was purchased from Santa Cruz Biotech (catalog number H-109). Mouse serum, Armenian hamster serum, rat serum, nonspecific mouse IgG, goat anti-Armenian hamster IgG, and Dylight 488– or Dylight 550–goat anti-rabbit and goat anti-mouse secondary antibodies were purchased from Jackson ImmunoResearch Laboratories. Rat anti-mouse PECAM, mouse anti-human CD18, rabbit anti-mouse collagen IV, rat anti-mouse MRP14, and goat anti-Armenian hamster IgG were directly conjugated with Dylight 488, DyLight 550, or Dylight 649 (Thermo Fisher Scientific), as indicated, according to the manufacturer's guidelines. Goat anti-rabbit–HRP and goat anti-mouse–HRP were purchased from BioRad.

Animals

All protocols involving mice were reviewed and approved by the Institutional Animal Care and Use Committee at Northwestern University (Public Health Service assurance number A328301). Mice were housed in the institutional animal facility operated by the Center for Comparative Medicine at Northwestern University and maintained according to standard Association for Assessment and Accreditation of Laboratory Animal Care methods. All experiments in this study used mice between 8 and 12 wk old. The C57BL/6 LysM-eGFP mouse strain (obtained from Dr. Paul Kubes, University of Calgary, Calgary, Canada) was described previously (Faust et al., 2000; Sullivan et al., 2016). Briefly, the myelomonocytic cells of these mice were rendered fluorescent by the insertion of eGFP in the lysozyme M (LysM) locus, under control of the LysM promoter. This allows for visualization of GFP^{hi} neutrophils and GFP^{low} monocytes/

macrophages. IQGAP1 knockout mice in the C57BL/6 background were a generous gift from Dr. Asrar Malik (University of Illinois at Chicago, Chicago, IL) and have been described elsewhere (Li et al., 2000; Urao et al., 2010).

Isolation of endothelial cells and primary human PBMCs

All procedures involving human subjects and human materials were approved by the Institutional Review Board of Northwestern University Feinberg School of Medicine. HUVECs were isolated from human umbilical cords as previously described (Muller et al., 1989; Muller and Luscinskas, 2008). At their second passage, isolated HUVECs were either cultured on three-dimensional (3D) type I collagen matrices (PureCol, Inamed Biomaterials; described in Muller and Luscinskas, 2008) or coverslip dishes (for the bead experiments; MatTek) and allowed to reach confluence before use (typically 2–3 d after seeding) to ensure the formation of high-quality basement membranes. To grow endothelial cells that behaved identically for the re-expression experiments, we used a well-characterized procedure to generate a stable iHUVEC line as described previously (Moses et al., 1999). In our hands as well as in other published studies, these cells have been shown to grow in stable monolayers, express appropriate levels of the relevant adhesion molecules, and support TEM similarly to unmodified HUVECs (Ancuta et al., 2003; Yang et al., 2005; Watson et al., 2015). PBMCs were harvested as described previously (Muller and Weigl, 1992; Muller and Luscinskas, 2008).

Cloning of IQGAP1 constructs and adenoviral transduction

shRNA constructs against the 3′ UTR of human IQGAP1 (National Center for Biotechnology Information accession no. NM_003870.3) KD1 5′-GGGCAATTCTGTTTGTGTAACTCCAGGTACCAGGAGTTACACAAACAGAATTGCCTTTTTT-3′ and KD2 5′-GGTGACAGTCATGTTCAAAGGAAGAGGTACCACTTCCTTTGAACATGACTGTCACTTTTTT-3′ under the control of the human U6 promotor were generated using site-directed mutagenesis by inverse PCR and the primers listed in Table 1 to replace the hairpin sequence of the nonspecific control pENTR4 vector (Invitrogen) described in Watson et al. (2015) (sequence 5′-ACTACCGTTGTTATAGGTGTTCAAGAGACACCTATAACAACGGTAGTTTTTT-3′). The corresponding IQGAP1 and control shRNA constructs were recombined with pAd/PL-DEST (Invitrogen) using LR clonase (Invitrogen) according to the manufacturer's guidelines. These vectors were then digested with PacI restriction enzyme (Fermentas; Thermo Fisher Scientific) and transfected into 293A cells to generate adenovirus for transduction according to the manufacturer's guidelines.

The FL IQGAP1 cDNA was obtained by PCR using human HT29 cell mRNA as a template with forward and reverse primers listed in Table 1. The PCR product was cloned into the Gateway donor vector pDONR201 (Invitrogen) as recommended by the manufacturer. The FL IQGAP1 construct was amplified using the primers detailed in Table 1 in the combination detailed in Table 2 and digested using SalI and XmaI. The resulting product was subcloned into a SalI/XmaI–digested pENTR4-GFP vector (a generous gift from Jonathan Jones, Northwestern University, Chicago, IL). The pENTR4-GFP vector was generated by combining the backbone of BamH1/NotI digested pENTR4 (Invitrogen) with the eGFP containing the BglII/NotI fragment of pEGFP-N1 (Clontech). pENTER4-mCherry was generated in exactly the same way from pmCherry-N1 (Clontech). To disrupt the internal PacI restriction site in IQGAP1 (required for subsequent virus production), the silent mutation A1632G was introduced using the primers indicated in Table 1 and site-directed mutagenesis by inverse PCR. This FL IQGAP1 construct (referred to here as FL) was used as the template to generate the IQGAP1 truncation constructs using the primers and combinations detailed in Tables 1 and 2. All forward primers were engineered to contain a Kozak sequence and a start codon; the reverse primers were designed to be in frame and without a stop codon between IQGAP1 and eGFP. Construct Δ4 (lacking nt 2,254–2,589, the internal deletion of domain 4 of IQGAP1) was generated using PCR with the primers in Table 2 and the IQGAP1-FL-GFP pENTR vector as a template. The resulting product was then ligated and transformed using standard methods. All constructs were sequenced to ensure the correct insertion and fidelity of the subcloning. The resulting C-terminal GFP-tagged constructs were recombined with the adenoviral pAd/CMV/V5-DEST vector (Invitrogen). The resulting vectors were digested with PacI and transfected into 293A cells, which were then to produce adenovirus according to the manufacturer's guidelines for transduction of the various constructs.

For adenoviral transduction of iHUVECs, cells were seeded on supported collagen gels at 10,000 cells/well. The following day, monolayers were washed three times with conditioned media and incubated with knockdown or control adenovirus in 100 µl of conditioned media overnight. Monolayers were then washed as before and incubated with the indicated rescue construct in 100 µl of conditioned media overnight. The media was then replaced with fresh media for 24 h before the cells were used in the experiments. With this scheme, the knockdown and reexpression constructs were transduced for 72 and 48 h, respectively, before the start of each assay. All experiments involving the knockdown (and reexpression, where indicated) were performed with this timing.

Western blotting

HUVECs or iHUVECs were grown on collagen gels and transduced as indicated and described above. After washing with PBS, the cells were lysed in 50 µl PBS containing 1% NP-40, 1× protease inhibitor cocktail (P8340; Sigma-Aldrich), and 1 mM PMSF (Sigma-Aldrich) for 5 min at room temperature (RT). The lysates were collected and pooled from two or three wells, mixed with 6× Laemmli loading buffer with β-mercaptoethanol, and heated at 60°C for 30 min. Equivalent amounts were loaded onto a 8% polyacrylamide gel and resolved using SDS-PAGE. Proteins were transferred to polyvinylidene difluoride membrane and detected using standard Western blotting techniques. The amount of virus needed to achieve expression levels for the constructs that was comparable to endogenous IQGAP1 expression level was determined empirically for each construct.

Quantification of LBRC size

Immunochemical quantification of LBRC size was performed as previously described (Feng et al., 2015) using the differential

accessibility of the LBRC to externally provided antibody at 37°C vs. 4°C followed by complete immunoprecipitation and quantitative scanning of Western blots.

Permeability assay

For permeability assays, endothelial cells were cultured on collagen gels as described above. Monolayers were washed with PBS and 100 µg/ml 10-kD rhodamine-Dextran (Sigma-Aldrich) was added to each well. Monolayers were then incubated at 37°C in 5% CO_2 for 1 h. After 1 h, monolayers were then washed extensively with PBS and the relative fluorescence intensity of rhodamine-dextran that had passed across the monolayers into the collagen gels was measured by a FilterMax F5 microplate reader (Molecular Devices). Indicated results are the mean fluorescence intensity of at least three independent experiments with at least replicates for each sample.

Immunofluorescence microscopy

Confluent HUVECs or iHUVECs were fixed in 2% paraformaldehyde for 20 min, washed three times with PBS, and blocked with blocking buffer (PBS with 5% BSA [Fraction V; Thermo Fisher Scientific] and 1% goat serum) was added for 30 min at RT. Cells were then incubated with primary antibody at 10 µg/ml in blocking buffer for 45 min at RT, washed extensively with PBS, and then incubated with secondary antibody at 4 µg/ml in blocking buffer for 45 min at RT protected from light. For the visualization of IQGAP1, cells were permeabilized before blocking for 4 min with 0.1% Triton X-100 (Sigma-Aldrich). Confocal images (all figures unless otherwise noted) were collected using an Ultraview VoX imaging system equipped with a Yokogawa CSU-1 spinning disk. Images were acquired with a 40× oil objective using Volocity software (numerical aperture [NA] 1.0). Widefield images (specifically Figs. 4 A and 5 C) were collected using a restoration workstation (DeltaVision 3D; Applied Precision) equipped with an inverted microscope (model IX70; Olympus) using a 60× oil objective (NA 1.42). Some widefield images (specifically Fig. 4 A) were processed using DeltaVision software and its associated constrained iterative deconvolution algorithm using a point spread function collected contemporaneously for each channel using standard fluorescence beads.

Analysis of junctional localization

Images from iHUVECs transduced with either control or IQGAP1 shRNA 1 and expressing the various IQGAP1 rescue constructs were analyzed to determine the enrichment of the various proteins at the junction. For each junctional analysis, a 20-µm line was drawn centered on and perpendicular to the junction and the pixel intensity along that line was recorded for each of channel. Suitable junctions were identified for analysis based on the continuity and intensity of VE-cadherin staining and without regard for the signal in the other channels. Although the images were all collected under the same settings, the individual lines still needed to be adjusted relative to the each other to account for variations in staining intensity (for PECAM and VE-cadherin) and expression (for the IQGAP1 constructs). For VE-cadherin and PECAM, the histogram plots were normalized to the maximum (which was also the midpoint of the junction). For the IQGAP1 constructs, the plot values were normalized to the cytoplasmic intensity distal to the junction. Note that this makes the intensities for the construct plots similar at the distal 0 µm and/or 20 µm ends of the plot but retains any meaningful differences at the junction in the middle.

Polystyrene bead coating

Polystyrene beads (average diameter, 3 µm) were coated as described previously (Sullivan et al., 2013; Weber et al., 2015). For the bead experiments, HUVEC monolayers were grown on fibronectin-coated coverslip dishes to confluence. The conjugated beads were diluted into preconditioned HUVEC media and allowed to settle on the cells and bind for 20 min to polystyrene beads. Monolayers were then washed with PBS, fixed with 4% paraformaldehyde and the indicated proteins visualized using confocal immunofluorescence. Images within each experiment were captured under identical settings and processed identically using ImageJ software to preserve any differences in relative intensities. Images were first background corrected by subtracting the background value (determined as the average pixel intensity in an off cell area) from the raw pixel intensity across the entire image. Beads were then analyzed using line scanning. Beads were score positive for enrichment if the IQGAP1 fluorescence intensity adjacent to the bead was ≥1.5-fold higher than the intensity several microns away from the bead. More than 300 beads were analyzed in three separate experiments were quantitated.

TEM and LBRC targeted recycling assays

TEM assays were performed on cytokine activated endothelial cells as previously described (Muller and Luscinskas, 2008). Imaging was performed with a Zeiss Ultraphot microscope with Nomarski optics and a SPOT Insight Color CCD (Diagnostic Instruments). TEM was analyzed by manually counting ≥100 cells per collagen gel and noting their position relative to the endothelial monolayer (above or below, with "above" defined as any monocyte having a majority of its cell body at or above the focal plane of the endothelial cell nuclei).

Visualization of LBRC during TEM (referred to as targeted recycling) was performed as described previously (Mamdouh et al., 2009; Watson et al., 2015; Weber et al., 2015). For this assay, we first tagged total PECAM (LBRC and surface) on cytokine-activated endothelial cells with anti-PECAM F(ab) fragments that are not function-blocking and then masked the surface pool with unlabeled $F(ab')_2$ secondary antibodies at 4°C. After adding PBMCs and fluorescently labeled $F(ab')_2$ secondary antibody, samples were warmed for 10 min to allow synchronized TEM. Because this assay is brief and performed under static conditions, most lymphocytes do not bind and are washed away. The relatively few lymphocytes that do bind are easily identified by their morphology and are not scored. During the 10-min incubation, monocytes bind and trigger the recruitment of the LBRC, which then exposes the previously unblocked primary epitopes contained within it. These epitopes can then be bound by the fluorescent secondary antibodies, and thus, when imaged using confocal microscopy, the recruitment of the LBRC

is observed as increased fluorescence signal adjacent to migrating monocytes (Fig. 3 A). Leukocytes are visualized by staining with Dylight 649–conjugated anti-CD18 after fixation. LBRC recruitment is scored by measuring the background-subtracted fluorescence signal next to the monocyte compared with the average background-subtracted signal at junctions several microns away from the monocyte. LBRC recruitment was scored as positive if at least two regions with a signal at least 1.5 times the uninvolved junction, although most leukocytes have multiple regions or an even ring of enrichment. Events that do not recruit the LBRC typically have a ratio of 1 ± 0.1; i.e., the signal around the leukocyte is not higher than the signal of the neighboring junctions.

Bone marrow chimeras

To focus on the role of endothelial cell IQGAP1 specifically, bone marrow chimeras were used for the animal studies described here using standard protocols (Duran-Struuck and Dysko, 2009; Mahajan et al., 2015). WT and IQGAP1 knockout mice were lethally irradiated with a 1,000-cGy dose using a Gammacell 40 Exactor ^{137}Cs irradiator and reconstituted with bone marrow from C57BL/6 WT mice (or LysM$^{+/GFP}$ heterozygous mice for the intravital studies). Bone marrow donors and recipients were always matched according to gender. Recipients recovered for 1 mo to allow for complete reconstitution of their bone marrow before being used in these experiments. Reconstitution was confirmed with PCR (for presence of the WT IQGAP1 and LysM-GFP alleles) and fluorescence imaging of a blood smear (for the presence of the GFP neutrophils).

Croton oil dermatitis model and immunofluorescence staining of whole-mount ears

Croton oil–induced inflammation was performed essentially as described previously (Schenkel et al., 2004; Watson et al., 2015; Sullivan et al., 2016) using 20 µl of 0.9% croton oil in a 4:1 solution of acetone/olive oil (carrier) and allowing 5 h to induce inflammation. The contralateral ear was treated with carrier only. After harvesting, fixing, permeablizing, and blocking, the ear leaflets were stained with 1 µg/ml anti-MRP14 conjugated to DyLight 488, 10 µg/ml anti-PECAM (clone 2H8) conjugated to DyLight 550, and 1 µg/ml anti-collagen IV conjugated to DyLight 649. Images were collected as above using a 40× oil-immersion lens (NA 1.0). Ears that received carrier alone were examined to ensure that the inflammatory stimulus was active and specific. For the inflamed ears, at least eight fields per ear were imaged, which typically corresponded to >100 neutrophils counted per mouse.

IVM of the mouse cremaster

Preparation of the cremaster muscle for visualization using fluorescence microscopy was performed essentially as described previously (Thompson et al., 2001; Sumagin and Sarelius, 2007; Woodfin et al., 2011; Sullivan et al., 2016). Briefly, male mice between 8 and 12 wk old were injected intrascrotally with 50 ng mouse recombinant IL-1β (R&D Systems) and 100 mg DyLight 550–conjugated nonblocking rat anti-mouse PECAM (clone 390) in a final volume of 100 µl 4 h before exteriorization and visualization of the cremaster muscle. The tissue was visualized using an Ultraview Vox imaging system equipped with a Yokogawa CSU-1 spinning disk and a 20× water-immersion objective (NA = 1.00). Images (Fig. 10 and Videos 1 and 2) were collected using Volocity software (Perkin Elmer) and analyzed using ImageJ (Schneider et al., 2012). Fields containing postcapillary venules with normal flow were identified using bright-field illumination. Ideal fields were those containing a relatively straight 30–50-µm postcapillary venule with robust steady flow. Three separate sets of images were collected for each field. First, a 3D stack in the red (anti-PECAM, endothelial junctions) channel was captured to determine the vessel dimensions. Then, in the green (LysM-GFP, neutrophils) channel, a 60-s, single-plane recording (one frame per second) was captured near the middle of the vessel to determine the rolling velocity and flux. Lastly, a 30–60-min recording (four frames per second) of both channels in 3D was captured to quantify TEM. After collecting the recordings, the field was examined again using bright-field illumination to check for any changes in flow rate. Fields that had slowed or stopped flow during the acquisition or that appeared to have changed upon bright-field illumination after the acquisition were not analyzed.

Image processing and data collection

The number of adherent neutrophils was calculated from the 60-s recording. Adherent neutrophils were identified as those that did not move more than one cell diameter (~5 µm) for ≥30 s during the recording (Sumagin et al., 2008, 2011). Although the recording only captured one plane (through the middle of the vessel), adherent and rolling neutrophils were easily identified in the adjacent, slightly out-of-focus planes by adjusting the contrast levels. The total number of adherent neutrophils per vessel surface area was calculated using the vessel dimensions and modeling the vessel as a cylinder with open ends (vessel surface area = πdl, where d is the average vessel diameter and l is the vessel length). Rolling velocity was calculated by manually tracking the distance individual neutrophils moved frame by frame for those that rolled uninterrupted for ≥10 frames; rolling velocity was only calculated from measurements collected while the neutrophil was actively rolling. Rolling flux was calculated by counting the number of neutrophils that rolled across an arbitrary point in the vessel during the 60-s recording and dividing by the total number (rollers and those free in the bloodstream) that passed the same point. TEM was calculated from the long 4D recordings. TEM events were defined as those in which the neutrophil traversed from clearly inside to clearly outside of the vessel and separated from it. Neutrophils were easily distinguished from monocytes based on morphology and intensity (GFPhi). Furthermore, neutrophils are the predominant leukocyte subset recruited at the early time point of 4 h after introduction of an inflammatory stimulus (Soehnlein et al., 2009).

In vivo vascular permeability

The Miles assay measuring the vascular leakage of Evans Blue was performed as described elsewhere (Schulte et al., 2011; Radu and Chernoff, 2013). Briefly, 100 µl of 10 mg/ml Evans Blue in

PBS was injected retro-orbitally. After 30 min, mice were sacrificed and tissue samples (one ear and a 1-cm circular piece of dorsal skin) were collected. Samples were weighed and then incubated with 0.5 ml formamide at 55°C for 24 h Absorbance at 620 nm of the supernatant was measured and the concentration of Evans Blue calculated using a standard curve.

Statistical analysis

All in vitro experiments with quantitation were performed independently at least three times with at least three replicates for each sample within each experiment. For the croton oil dermatitis experiments, each experiment contained at least three mice for each condition. Average values within each experiment were averaged between experiments to produce the data, and standard deviations shown here. For the IVM experiments, the data shown were compiled from three mice for each condition with one recording for each mouse. For the transmigration assays, the values for the replicates were averaged together within each experiment. The average and standard deviation of these averages is shown in the figures. For each experimental, P values were calculated from the average values using the Student's *t* test with a Bonferroni correction for unpaired observations. Statistical differences are denoted by asterisks and denote P values that can be found in the corresponding figure legend.

Online supplemental material

Supplemental figures show the expression and localization of VE-cadherin (Fig. S1), ICAM-1 (Fig. S2), CD99 (Fig. S3), actin (Fig. S4), and microtubules (Fig. S5) that are involved in various steps in leukocyte recruitment and transmigration. None of the molecules examined (VE-cadherin, ICAM, CD99, the actin cytoskeleton, or the microtubule network) were significantly altered in their abundance or distribution as a result of IQGAP1 knockdown or the reexpression of the relevant IQGAP1 constructs. Videos 1 and 2 are representative recordings of in-vivo leukocyte recruitment and TEM in WT and IQGAP1 knockout mice.

Acknowledgments

We would like to thank Clifford D. Carpenter for assistance with experiments; Laetitia Gorisse, Andrew Hedman, Chase Morgan, Gong Feng, and Sumana Sanyal for insightful discussions; Dr. David Klumpp (Northwestern University Feinberg School of Medicine, Chicago, IL) for the generous donation of the retrovirus used to immortalize HUVECs; and Dr. Asrar Malik (University of Illinois at Chicago, Chicago, IL) for providing the IQGAP1 knockout mice.

This work was supported by the National Institutes of Health (grant F32 AI084454 to D.P. Sullivan; grants R01 HL046849, R21 HL102519, and R37 HL064774 to W.A. Muller; and grants F30 HL134202 and T32 GM8152 to P.J. Dalal), an Alpha Omega Alpha Carolyn L. Kuckein Student Research Fellowship (to P.J. Dalal), the National Institutes of Health Intramural Research Program funding (D.B. Sacks), and National Institutes of Health National Institute of General Medical Sciences grant R01 GM087575 (to G. Kreitzer).

The authors declare no competing financial interests.

Author contributions: D.P. Sullivan and W.A. Muller conceived and designed this study; F. Jaulin and G. Kreitzer cloned the initial IQGAP1 construct; D.P. Sullivan and P.J. Dalal performed the data collection and analysis; D.P. Sullivan drafted the manuscript; and D.P. Sullivan, P.J. Dalal, F. Jaulin, G. Kreitzer, D.B. Sacks, and W.A. Muller all contributed to the revision of the manuscript and approved its final version for publication.

Submitted: 2 January 2019
Revised: 10 June 2019
Accepted: 3 July 2019

References

Abel, A.M., K.M. Schuldt, K. Rajasekaran, D. Hwang, M.J. Riese, S. Rao, M.S. Thakar, and S. Malarkannan. 2015. IQGAP1: insights into the function of a molecular puppeteer. *Mol. Immunol.* 65:336–349. https://doi.org/10.1016/j.molimm.2015.02.012

Ali, J., F. Liao, E. Martens, and W.A. Muller. 1997. Vascular endothelial cadherin (VE-cadherin): cloning and role in endothelial cell-cell adhesion. *Microcirculation.* 4:267–277. https://doi.org/10.3109/10739689709146790

Ancuta, P., R. Rao, A. Moses, A. Mehle, S.K. Shaw, F.W. Luscinskas, and D. Gabuzda. 2003. Fractalkine preferentially mediates arrest and migration of CD16+ monocytes. *J. Exp. Med.* 197:1701–1707. https://doi.org/10.1084/jem.20022156

Bähler, M., and A. Rhoads. 2002. Calmodulin signaling via the IQ motif. *FEBS Lett.* 513:107–113. https://doi.org/10.1016/S0014-5793(01)03239-2

Bashour, A.M., A.T. Fullerton, M.J. Hart, and G.S. Bloom. 1997. IQGAP1, a Rac- and Cdc42-binding protein, directly binds and cross-links microfilaments. *J. Cell Biol.* 137:1555–1566. https://doi.org/10.1083/jcb.137.7.1555

Bogen, S., J. Pak, M. Garifallou, X. Deng, and W.A. Muller. 1994. Monoclonal antibody to murine PECAM-1 (CD31) blocks acute inflammation in vivo. *J. Exp. Med.* 179:1059–1064. https://doi.org/10.1084/jem.179.3.1059

Briggs, M.W., and D.B. Sacks. 2003a. IQGAP1 as signal integrator: Ca2+, calmodulin, Cdc42 and the cytoskeleton. *FEBS Lett.* 542:7–11. https://doi.org/10.1016/S0014-5793(03)00333-8

Briggs, M.W., and D.B. Sacks. 2003b. IQGAP proteins are integral components of cytoskeletal regulation. *EMBO Rep.* 4:571–574. https://doi.org/10.1038/sj.embor.embor867

Cao, D., Z. Su, W. Wang, H. Wu, X. Liu, S. Akram, B. Qin, J. Zhou, X. Zhuang, G. Adams, et al. 2015. Signaling Scaffold Protein IQGAP1 Interacts with Microtubule Plus-end Tracking Protein SKAP and Links Dynamic Microtubule Plus-end to Steer Cell Migration. *J. Biol. Chem.* 290:23766–23780. https://doi.org/10.1074/jbc.M115.673517

Caride, A.J., R.D. Bennett, and E.E. Strehler. 2010. Kinetic analysis reveals differences in the binding mechanism of calmodulin and calmodulin-like protein to the IQ motifs of myosin-10. *Biochemistry.* 49:8105–8116. https://doi.org/10.1021/bi100644q

Cyrus, B.F., and W.A. Muller. 2016. A Unique Role for Endothelial Cell Kinesin Light Chain 1, Variant 1 in Leukocyte Transendothelial Migration. *Am. J. Pathol.* 186:1375–1386. https://doi.org/10.1016/j.ajpath.2016.01.011

Dasgupta, B., E. Dufour, Z. Mamdouh, and W. Muller. 2009. A novel and critical role for tyrosine 663 in PECAM trafficking and transendothelial migration. *J. Immunol.* 182:5041–5051. https://doi.org/10.4049/jimmunol.0803192

Duran-Struuck, R., and R.C. Dysko. 2009. Principles of bone marrow transplantation (BMT): providing optimal veterinary and husbandry care to irradiated mice in BMT studies. *J. Am. Assoc. Lab. Anim. Sci.* 48:11–22.

Faust, N., F. Varas, L.M. Kelly, S. Heck, and T. Graf. 2000. Insertion of enhanced green fluorescent protein into the lysozyme gene creates mice with green fluorescent granulocytes and macrophages. *Blood.* 96:719–726.

Feng, G., D.P. Sullivan, F. Han, and W.A. Muller. 2015. Segregation of VE-cadherin from the LBRC depends on the ectodomain sequence required for homophilic adhesion. *J. Cell Sci.* 128:576–588. https://doi.org/10.1242/jcs.159053

Firestein, G.S., and I.B. McInnes. 2017. Immunopathogenesis of Rheumatoid Arthritis. *Immunity.* 46:183–196. https://doi.org/10.1016/j.immuni.2017.02.006

Fukata, M., S. Kuroda, K. Fujii, T. Nakamura, I. Shoji, Y. Matsuura, K. Okawa, A. Iwamatsu, A. Kikuchi, and K. Kaibuchi. 1997. Regulation of cross-linking of actin filament by IQGAP1, a target for Cdc42. *J. Biol. Chem.* 272: 29579–29583. https://doi.org/10.1074/jbc.272.47.29579

Gerhardt, T., and K. Ley. 2015. Monocyte trafficking across the vessel wall. *Cardiovasc. Res.* 107:321–330. https://doi.org/10.1093/cvr/cvv147

Gonzalez, A.M., B.F. Cyrus, and W.A. Muller. 2016. Targeted Recycling of the Lateral Border Recycling Compartment Precedes Adherens Junction Dissociation during Transendothelial Migration. *Am. J. Pathol.* 186: 1387–1402. https://doi.org/10.1016/j.ajpath.2016.01.010

Grigoriadis, N., and V. van Pesch. ParadigMS Group. 2015. A basic overview of multiple sclerosis immunopathology. *Eur. J. Neurol.* 22(Suppl 2):3–13. https://doi.org/10.1111/ene.12798

Hedman, A.C., J.M. Smith, and D.B. Sacks. 2015. The biology of IQGAP proteins: beyond the cytoskeleton. *EMBO Rep.* 16:427–446. https://doi.org/10.15252/embr.201439834

Huang, A.J., J.E. Manning, T.M. Bandak, M.C. Ratau, K.R. Hanser, and S.C. Silverstein. 1993. Endothelial cell cytosolic free calcium regulates neutrophil migration across monolayers of endothelial cells. *J. Cell Biol.* 120: 1371–1380. https://doi.org/10.1083/jcb.120.6.1371

Jang, D.J., B. Ban, and J.A. Lee. 2011. Characterization of novel calmodulin binding domains within IQ motifs of IQGAP1. *Mol. Cells.* 32:511–518. https://doi.org/10.1007/s10059-011-0109-4

Joyal, J.L., R.S. Annan, Y.D. Ho, M.E. Huddleston, S.A. Carr, M.J. Hart, and D.B. Sacks. 1997. Calmodulin modulates the interaction between IQGAP1 and Cdc42. Identification of IQGAP1 by nanoelectrospray tandem mass spectrometry. *J. Biol. Chem.* 272:15419–15425. https://doi.org/10.1074/jbc.272.24.15419

Li, Z., and D.B. Sacks. 2003. Elucidation of the interaction of calmodulin with the IQ motifs of IQGAP1. *J. Biol. Chem.* 278:4347–4352. https://doi.org/10.1074/jbc.M208579200

Li, S., Q. Wang, A. Chakladar, R.T. Bronson, and A. Bernards. 2000. Gastric hyperplasia in mice lacking the putative Cdc42 effector IQGAP1. *Mol. Cell. Biol.* 20:697–701. https://doi.org/10.1128/MCB.20.2.697-701.2000

Li, Z., S.H. Kim, J.M. Higgins, M.B. Brenner, and D.B. Sacks. 1999. IQGAP1 and calmodulin modulate E-cadherin function. *J. Biol. Chem.* 274: 37885–37892. https://doi.org/10.1074/jbc.274.53.37885

Liao, F., J. Ali, T. Greene, and W.A. Muller. 1997. Soluble domain 1 of platelet-endothelial cell adhesion molecule (PECAM) is sufficient to block transendothelial migration in vitro and in vivo. *J. Exp. Med.* 185: 1349–1357. https://doi.org/10.1084/jem.185.7.1349

Liu, J., V.B. Kurella, L. LeCour Jr., T. Vanagunas, and D.K. Worthylake. 2016. The IQGAP1 N-Terminus Forms Dimers, and the Dimer Interface Is Required for Binding F-Actin and Calcium-Bound Calmodulin. *Biochemistry.* 55:6433–6444. https://doi.org/10.1021/acs.biochem.6b00745

Mahajan, M.M., B. Cheng, A.I. Beyer, U.S. Mulvaney, M.B. Wilkinson, M.E. Fomin, and M.O. Muench. 2015. A quantitative assessment of the content of hematopoietic stem cells in mouse and human endosteal-bone marrow: a simple and rapid method for the isolation of mouse central bone marrow. *BMC Hematol.* 15:9. https://doi.org/10.1186/s12878-015-0031-7

Malarkannan, S., A. Awasthi, K. Rajasekaran, P. Kumar, K.M. Schuldt, A. Bartoszek, N. Manoharan, N.K. Goldner, C.M. Umhoefer, and M.S. Thakar. 2012. IQGAP1: a regulator of intracellular spacetime relativity. *J. Immunol.* 188:2057–2063. https://doi.org/10.4049/jimmunol.1102439

Mamdouh, Z., X. Chen, L.M. Pierini, F.R. Maxfield, and W.A. Muller. 2003. Targeted recycling of PECAM from endothelial surface-connected compartments during diapedesis. *Nature.* 421:748–753. https://doi.org/10.1038/nature01300

Mamdouh, Z., G.E. Kreitzer, and W.A. Muller. 2008. Leukocyte transmigration requires kinesin-mediated microtubule-dependent membrane trafficking from the lateral border recycling compartment. *J. Exp. Med.* 205:951–966. https://doi.org/10.1084/jem.20072328

Mamdouh, Z., A. Mikhailov, and W.A. Muller. 2009. Transcellular migration of leukocytes is mediated by the endothelial lateral border recycling compartment. *J. Exp. Med.* 206:2795–2808. https://doi.org/10.1084/jem.20082745

Mateer, S.C., A.E. McDaniel, V. Nicolas, G.M. Habermacher, M.J. Lin, D.A. Cromer, M.E. King, and G.S. Bloom. 2002. The mechanism for regulation of the F-actin binding activity of IQGAP1 by calcium/calmodulin. *J. Biol. Chem.* 277:12324–12333. https://doi.org/10.1074/jbc.M109535200

Moses, A.V., K.N. Fish, R. Ruhl, P.P. Smith, J.G. Strussenberg, L. Zhu, B. Chandran, and J.A. Nelson. 1999. Long-term infection and transformation of dermal microvascular endothelial cells by human herpesvirus 8. *J. Virol.* 73:6892–6902.

Muller, W.A. 2011. Mechanisms of leukocyte transendothelial migration. *Annu. Rev. Pathol.* 6:323–344. https://doi.org/10.1146/annurev-pathol-011110-130224

Muller, W.A. 2016a. Localized signals that regulate transendothelial migration. *Curr. Opin. Immunol.* 38:24–29. https://doi.org/10.1016/j.coi.2015.10.006

Muller, W.A. 2016b. Transendothelial migration: unifying principles from the endothelial perspective. *Immunol. Rev.* 273:61–75. https://doi.org/10.1111/imr.12443

Muller, W.A., and F.W. Luscinskas. 2008. Assays of transendothelial migration in vitro. *Methods Enzymol.* 443:155–176. https://doi.org/10.1016/S0076-6879(08)02009-0

Muller, W.A., and S.A. Weigl. 1992. Monocyte-selective transendothelial migration: dissection of the binding and transmigration phases by an in vitro assay. *J. Exp. Med.* 176:819–828. https://doi.org/10.1084/jem.176.3.819

Muller, W.A., C.M. Ratti, S.L. McDonnell, and Z.A. Cohn. 1989. A human endothelial cell-restricted, externally disposed plasmalemmal protein enriched in intercellular junctions. *J. Exp. Med.* 170:399–414. https://doi.org/10.1084/jem.170.2.399

Muller, W.A., S.A. Weigl, X. Deng, and D.M. Phillips. 1993. PECAM-1 is required for transendothelial migration of leukocytes. *J. Exp. Med.* 178: 449–460. https://doi.org/10.1084/jem.178.2.449

Nakhaei-Nejad, M., Q.X. Zhang, and A.G. Murray. 2010. Endothelial IQGAP1 regulates efficient lymphocyte transendothelial migration. *Eur. J. Immunol.* 40:204–213. https://doi.org/10.1002/eji.200839214

Nussinov, R., and H. Jang. 2014. Dynamic multiprotein assemblies shape the spatial structure of cell signaling. *Prog. Biophys. Mol. Biol.* 116:158–164. https://doi.org/10.1016/j.pbiomolbio.2014.07.002

Pathmanathan, S., S.F. Elliott, S. McSwiggen, B. Greer, P. Harriott, G.B. Irvine, and D.J. Timson. 2008. IQ motif selectivity in human IQGAP1: binding of myosin essential light chain and S100B. *Mol. Cell. Biochem.* 318:43–51. https://doi.org/10.1007/s11010-008-9855-9

Pelikan-Conchaudron, A., C. Le Clainche, D. Didry, and M.F. Carlier. 2011. The IQGAP1 protein is a calmodulin-regulated barbed end capper of actin filaments: possible implications in its function in cell migration. *J. Biol. Chem.* 286:35119–35128. https://doi.org/10.1074/jbc.M111.258772

Radu, M., and J. Chernoff. 2013. An in vivo assay to test blood vessel permeability. *J. Vis. Exp.* (73):e50062.

Ren, J.G., Z. Li, D.L. Crimmins, and D.B. Sacks. 2005. Self-association of IQGAP1: characterization and functional sequelae. *J. Biol. Chem.* 280: 34548–34557. https://doi.org/10.1074/jbc.M507321200

Schenkel, A.R., Z. Mamdouh, X. Chen, R.M. Liebman, and W.A. Muller. 2002. CD99 plays a major role in the migration of monocytes through endothelial junctions. *Nat. Immunol.* 3:143–150. https://doi.org/10.1038/ni749

Schenkel, A.R., T.W. Chew, and W.A. Muller. 2004. Platelet endothelial cell adhesion molecule deficiency or blockade significantly reduces leukocyte emigration in a majority of mouse strains. *J. Immunol.* 173: 6403–6408. https://doi.org/10.4049/jimmunol.173.10.6403

Schneider, C.A., W.S. Rasband, and K.W. Eliceiri. 2012. NIH Image to ImageJ: 25 years of image analysis. *Nat. Methods.* 9:671–675. https://doi.org/10.1038/nmeth.2089

Schnoor, M. 2015. Endothelial actin-binding proteins and actin dynamics in leukocyte transendothelial migration. *J. Immunol.* 194:3535–3541. https://doi.org/10.4049/jimmunol.1403250

Schnoor, M., F.P. Lai, A. Zarbock, R. Kläver, C. Polaschegg, D. Schulte, H.A. Weich, J.M. Oelkers, K. Rottner, and D. Vestweber. 2011. Cortactin deficiency is associated with reduced neutrophil recruitment but increased vascular permeability in vivo. *J. Exp. Med.* 208:1721–1735. https://doi.org/10.1084/jem.20101920

Schulte, D., V. Küppers, N. Dartsch, A. Broermann, H. Li, A. Zarbock, O. Kamenyeva, F. Kiefer, A. Khandoga, S. Massberg, and D. Vestweber. 2011. Stabilizing the VE-cadherin-catenin complex blocks leukocyte extravasation and vascular permeability. *EMBO J.* 30:4157–4170. https://doi.org/10.1038/emboj.2011.304

Shaw, S.K., P.S. Bamba, B.N. Perkins, and F.W. Luscinskas. 2001. Real-time imaging of vascular endothelial-cadherin during leukocyte transmigration across endothelium. *J. Immunol.* 167:2323–2330. https://doi.org/10.4049/jimmunol.167.4.2323

Soehnlein, O., L. Lindbom, and C. Weber. 2009. Mechanisms underlying neutrophil-mediated monocyte recruitment. *Blood.* 114:4613–4623. https://doi.org/10.1182/blood-2009-06-221630

Su, W.H., H.I. Chen, J.P. Huang, and C.J. Jen. 2000. Endothelial [Ca(2+)](i) signaling during transmigration of polymorphonuclear leukocytes. *Blood.* 96:3816–3822.

Sullivan, D.P., and W.A. Muller. 2014. Neutrophil and monocyte recruitment by PECAM, CD99, and other molecules via the LBRC. *Semin. Immunopathol.* 36:193–209. https://doi.org/10.1007/s00281-013-0412-6

Sullivan, D.P., M.A. Seidman, and W.A. Muller. 2013. Poliovirus receptor (CD155) regulates a step in transendothelial migration between PECAM and CD99. *Am. J. Pathol.* 182:1031–1042. https://doi.org/10.1016/j.ajpath.2012.11.037

Sullivan, D.P., C. Rüffer, and W.A. Muller. 2014. Isolation of the lateral border recycling compartment using a diaminobenzidine-induced density shift. *Traffic.* 15:1016–1029. https://doi.org/10.1111/tra.12184

Sullivan, D.P., R.L. Watson, and W.A. Muller. 2016. 4D intravital microscopy uncovers critical strain differences for the roles of PECAM and CD99 in leukocyte diapedesis. *Am. J. Physiol. Heart Circ. Physiol.* 311:H621–H632. https://doi.org/10.1152/ajpheart.00289.2016

Sumagin, R., and I.H. Sarelius. 2007. A role for ICAM-1 in maintenance of leukocyte-endothelial cell rolling interactions in inflamed arterioles. *Am. J. Physiol. Heart Circ. Physiol.* 293:H2786–H2798. https://doi.org/10.1152/ajpheart.00720.2007

Sumagin, R., E. Lomakina, and I.H. Sarelius. 2008. Leukocyte-endothelial cell interactions are linked to vascular permeability via ICAM-1-mediated signaling. *Am. J. Physiol. Heart Circ. Physiol.* 295:H969–H977. https://doi.org/10.1152/ajpheart.00400.2008

Sumagin, R., J.M. Kuebel, and I.H. Sarelius. 2011. Leukocyte rolling and adhesion both contribute to regulation of microvascular permeability to albumin via ligation of ICAM-1. *Am. J. Physiol. Cell Physiol.* 301:C804–C813. https://doi.org/10.1152/ajpcell.00135.2011

Thompson, R.D., K.E. Noble, K.Y. Larbi, A. Dewar, G.S. Duncan, T.W. Mak, and S. Nourshargh. 2001. Platelet-endothelial cell adhesion molecule-1 (PECAM-1)-deficient mice demonstrate a transient and cytokine-specific role for PECAM-1 in leukocyte migration through the perivascular basement membrane. *Blood.* 97:1854–1860. https://doi.org/10.1182/blood.V97.6.1854

Tian, Y., X. Tian, G. Gawlak, J.J. O'Donnell III, D.B. Sacks, and A.A. Birukova. 2014. IQGAP1 regulates endothelial barrier function via EB1-cortactin cross talk. *Mol. Cell. Biol.* 34:3546–3558. https://doi.org/10.1128/MCB.00248-14

Tian, Y., X. Tian, G. Gawlak, N. Sarich, D.B. Sacks, A.A. Birukova, and K.G. Birukov. 2016. Role of IQGAP1 in endothelial barrier enhancement caused by OxPAPC. *Am. J. Physiol. Lung Cell. Mol. Physiol.* 311:L800–L809.

Urao, N., M. Razvi, J. Oshikawa, R.D. McKinney, R. Chavda, W.F. Bahou, T. Fukai, and M. Ushio-Fukai. 2010. IQGAP1 is involved in post-ischemic neovascularization by regulating angiogenesis and macrophage infiltration. *PLoS One.* 5:e13440. https://doi.org/10.1371/journal.pone.0013440

Usatyuk, P.V., I.A. Gorshkova, D. He, Y. Zhao, S.K. Kalari, J.G. Garcia, and V. Natarajan. 2009. Phospholipase D-mediated activation of IQGAP1 through Rac1 regulates hyperoxia-induced p47phox translocation and reactive oxygen species generation in lung endothelial cells. *J. Biol. Chem.* 284:15339–15352. https://doi.org/10.1074/jbc.M109.005439

van Buul, J.D., M.J. Allingham, T. Samson, J. Meller, E. Boulter, R. García-Mata, and K. Burridge. 2007. RhoG regulates endothelial apical cup assembly downstream from ICAM1 engagement and is involved in leukocyte trans-endothelial migration. *J. Cell Biol.* 178:1279–1293. https://doi.org/10.1083/jcb.200612053

van Rijssel, J., J. Kroon, M. Hoogenboezem, F.P. van Alphen, R.J. de Jong, E. Kostadinova, D. Geerts, P.L. Hordijk, and J.D. van Buul. 2012. The Rho-guanine nucleotide exchange factor Trio controls leukocyte transendothelial migration by promoting docking structure formation. *Mol. Biol. Cell.* 23:2831–2844. https://doi.org/10.1091/mbc.e11-11-0907

Vestweber, D., F. Wessel, and A.F. Nottebaum. 2014. Similarities and differences in the regulation of leukocyte extravasation and vascular permeability. *Semin. Immunopathol.* 36:177–192. https://doi.org/10.1007/s00281-014-0419-7

Watanabe, T., S. Wang, J. Noritake, K. Sato, M. Fukata, M. Takefuji, M. Nakagawa, N. Izumi, T. Akiyama, and K. Kaibuchi. 2004. Interaction with IQGAP1 links APC to Rac1, Cdc42, and actin filaments during cell polarization and migration. *Dev. Cell.* 7:871–883. https://doi.org/10.1016/j.devcel.2004.10.017

Watanabe, T., S. Wang, and K. Kaibuchi. 2015. IQGAPs as Key Regulators of Actin-cytoskeleton Dynamics. *Cell Struct. Funct.* 40:69–77. https://doi.org/10.1247/csf.15003

Watson, R.L., J. Buck, L.R. Levin, R.C. Winger, J. Wang, H. Arase, and W.A. Muller. 2015. Endothelial CD99 signals through soluble adenylyl cyclase and PKA to regulate leukocyte transendothelial migration. *J. Exp. Med.* 212:1021–1041. https://doi.org/10.1084/jem.20150354

Weber, E.W., F. Han, M. Tauseef, L. Birnbaumer, D. Mehta, and W.A. Muller. 2015. TRPC6 is the endothelial calcium channel that regulates leukocyte transendothelial migration during the inflammatory response. *J. Exp. Med.* 212:1883–1899. https://doi.org/10.1084/jem.20150353

Weissbach, L., A. Bernards, and D.W. Herion. 1998. Binding of myosin essential light chain to the cytoskeleton-associated protein IQGAP1. *Biochem. Biophys. Res. Commun.* 251:269–276. https://doi.org/10.1006/bbrc.1998.9371

Wessel, F., M. Winderlich, M. Holm, M. Frye, R. Rivera-Galdos, M. Vockel, R. Linnepe, U. Ipe, A. Stadtmann, A. Zarbock, et al. 2014. Leukocyte extravasation and vascular permeability are each controlled in vivo by different tyrosine residues of VE-cadherin. *Nat. Immunol.* 15:223–230. https://doi.org/10.1038/ni.2824

White, C.D., H.H. Erdemir, and D.B. Sacks. 2012. IQGAP1 and its binding proteins control diverse biological functions. *Cell. Signal.* 24:826–834. https://doi.org/10.1016/j.cellsig.2011.12.005

Winger, R.C., J.E. Koblinski, T. Kanda, R.M. Ransohoff, and W.A. Muller. 2014. Rapid remodeling of tight junctions during paracellular diapedesis in a human model of the blood-brain barrier. *J. Immunol.* 193:2427–2437. https://doi.org/10.4049/jimmunol.1400700

Woodfin, A., M.B. Voisin, M. Beyrau, B. Colom, D. Caille, F.M. Diapouli, G.B. Nash, T. Chavakis, S.M. Albelda, G.E. Rainger, et al. 2011. The junctional adhesion molecule JAM-C regulates polarized transendothelial migration of neutrophils in vivo. *Nat. Immunol.* 12:761–769. https://doi.org/10.1038/ni.2062

Wright, S.D., P.E. Rao, W.C. Van Voorhis, L.S. Craigmyle, K. Iida, M.A. Talle, E.F. Westberg, G. Goldstein, and S.C. Silverstein. 1983. Identification of the C3bi receptor of human monocytes and macrophages by using monoclonal antibodies. *Proc. Natl. Acad. Sci. USA.* 80:5699–5703. https://doi.org/10.1073/pnas.80.18.5699

Yang, L., R.M. Froio, T.E. Sciuto, A.M. Dvorak, R. Alon, and F.W. Luscinskas. 2005. ICAM-1 regulates neutrophil adhesion and transcellular migration of TNF-alpha-activated vascular endothelium under flow. *Blood.* 106:584–592. https://doi.org/10.1182/blood-2004-12-4942